JOURNAL OF GEOPHYSICAL RESEARCH, VOL. 112, B05408, doi:10.1029/2006JB004502, 2007

Click Here for Full Article

Thermal cracking and the deep hydration of oceanic lithosphere: A key to the generation of plate tectonics?

Jun Korenaga[1]

Received 14 May 2006; revised 30 October 2006; accepted 15 December 2006; published 10 May 2007.

[1] The development of transient thermal stress in suboceanic mantle is investigated on the basis of two-dimensional thermoviscoelastic models incorporating composite rheology appropriate for dry oceanic lithosphere. Thermal stress is shown to be sufficiently high to deeply fracture the coldest part of lithosphere, e.g., to the depth of at least ~30 km (and possibly down to ~50 km) in 100-Ma-old lithosphere. The release of thermal stress by tension cracking is limited to the vicinity of cracks, and the cascade crack system is suggested to be required given the finite fracture strength of mantle materials. Possible physical and chemical consequences of deep thermal cracking are also discussed. The rheological evolution of oceanic lithosphere is likely to be affected by thermal cracking and subsequent serpentinization, which introduces the localized zones of weakness in the otherwise stiffest part of lithosphere. This localized weakening may help to explain why plate tectonic convection, not stagnant lid convection, operates in Earth's mantle.

Citation: Korenaga, J. (2007), Thermal cracking and the deep hydration of oceanic lithosphere: A key to the generation of plate tectonics?, *J. Geophys. Res.*, *112*, B05408, doi:10.1029/2006JB004502.

1. Introduction

[2] The operation of plate tectonics is what distinguishes Earth from other terrestrial planets and perhaps the most puzzling aspect of mantle dynamics. Why convection in Earth's mantle gives rise to plate tectonics is not obvious [e.g., *Bercovici et al.*, 2000; *Tackley*, 2000; *Schubert et al.*, 2001]. The top thermal boundary layer is supposed to be very stiff because the viscosity of silicate rocks is strongly temperature-dependent [e.g., *Weertman*, 1970; *Karato and Wu*, 1993]. This temperature dependency is so strong that the so-called stagnant lid convection should be the most likely mode of mantle convection [*Solomatov*, 1995] (Figure 1); the entire surface should be covered by just one single plate, not by a number of rigid plates as one can readily recognize in the velocity field of Earth's surface. In order to generate plate tectonics, therefore there must exist some mechanism to compensate temperature-dependent viscosity, but what this mechanism could be is currently unresolved [e.g., *Bercovici*, 2003].

[3] At shallow depths, of course, rocks can deform by brittle fracture, but the top thermal boundary layer is still too strong. The yield stress envelope, as often used to discuss the strength of lithosphere, is useful to illustrate this point. Here, and also for the rest of this paper, I focus on the rheological structure of oceanic lithosphere, and the term "lithosphere" is used to denote the top thermal boundary layer of the convecting mantle. As the thickness of normal oceanic crust is only ~6 km, this crustal layer is neglected for the sake of simplicity when discussing oceanic lithosphere. Figure 2 shows the thermal and rheological structure expected for 100-Ma-old oceanic lithosphere. The top 50 km is below ~600°C. Because melting beneath mid-ocean ridges dehydrates residual mantle, this shallow part of lithosphere is expected to be dry, with $C_{H_2O} \ll 10$ ppm H/Si [*Hirth and Kohlstedt*, 1996]. This dehydrated nature of shallow upper mantle has also been supported by a magnetotelluric survey conducted at the East Pacific Rise [*Evans et al.*, 2005]. Assuming the dislocation creep of dry olivine, therefore effective viscosity and corresponding stress are calculated for a typical tectonic strain rate of 10^{-15} s^{-1}. Because the temperature dependency of mantle viscosity takes the Arrhenius form, effective viscosity increases superexponentially as temperature decreases nearly linearly (Figure 2b). Similarly, yield stress for dislocation creep increases very quickly with decreasing temperature, exceeding 1 GPa at the depth of ~45 km (Figure 2b).

[4] On the other hand, Byerlee's rule provides the minimum yield stress for brittle failure, which quickly increases with depth, exceeding 1 GPa at the depth of ~10 km in case of thrust faulting, with the friction coefficient of 0.8 [*Byerlee*, 1978]. Note that Byerlee's rule, which is relatively insensitive to lithology as well as roughness, constrains the stress supported by frictional sliding, and thus this stress is scale-independent. This should not be confused with fracture strength. Fracture strength depends on the size of intrinsic flaws, so larger samples would break more easily than smaller samples. Byerlee's rule determines the stress that can be supported by pervasively fractured rocks, providing the lowest possible fracture strength [e.g., *Scholz*, 2002]. Therefore, for the depth range of 10–45 km, oceanic lithosphere of this age is too stiff to be deformed by any

[1]Department of Geology and Geophysics, Yale University, New Haven, Connecticut, USA.

0148-0227/07/2006JB004502$09.00

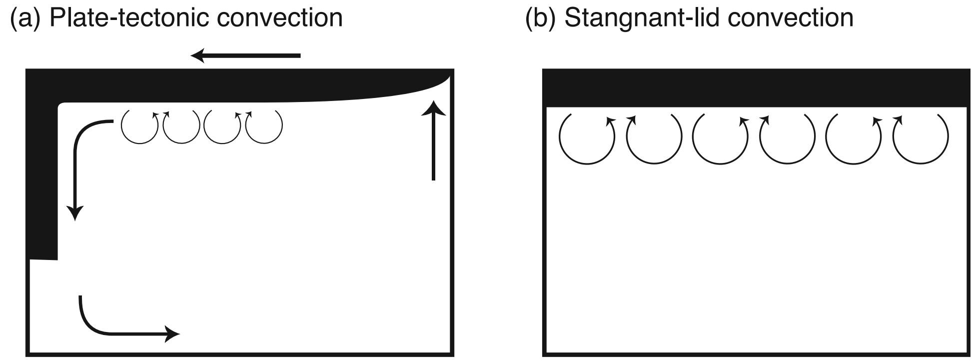

Figure 1. Two contrasting styles of mantle convection: (a) plate tectonic convection, in which the top thermal boundary layer is continuously recycled back to the mantle, and (b) stagnant lid convection, in which the entire surface is one immobile rigid plate.

reasonable tectonic stress, resulting in a fatal bottleneck for the operation of plate tectonics. Material strength between brittle failure and plastic creep could be considerably weaker than suggested by the simple combination of Byerlee's rule and ductile flow law as done in the above, but the currently available estimate suggests that yield strength for this "semibrittle" regime is still on the order of 600–800 MPa [*Kohlstedt et al.*, 1995].

[5] It is known that the self-consistent numerical modeling of plate tectonics (i.e., plate tectonics naturally arising from buoyancy distribution and given rheology, not imposed by boundary conditions) is impossible with such high yield stress [e.g., *Moresi and Solomatov*, 1998; *Richards et al.*, 2001; *Solomatov*, 2004]. In all of previous attempts to simulate plate tectonics in a self-consistent fashion, therefore mantle rheology is modified in one way or another (e.g., by reducing the friction coefficient by an order of magnitude [e.g., *Moresi and Solomatov*, 1998]) so that the maximum yield strength is limited to ~100 MPa (Figure 2c). This approach may be defendable because the study of the San Andreas fault has suggested that Byerlee's may not be applicable at crustal scales [e.g., *Lachenbruch and Sass*, 1980; *Scholz*, 2000]. Byerlee's rule, however, appears to be valid well beyond laboratory conditions [*Brudy et al.*, 1997; *Scholz*, 2002], and even if the San Andreas fault were weak for some reasons, the same argument may not apply to oceanic lithosphere for two reasons. First, the thickness of continental crust around the San Andreas fault is ~30 km, considerably thicker than normal oceanic crust, and because of this, the yield stress profile expected for continental lithosphere is substantially subdued [e.g., *Kohlstedt et al.*, 1995]. Second, the friction coefficient could be lowered by assuming the presence of water, which is reasonable for continental crust, but not for oceanic lithosphere. Whereas

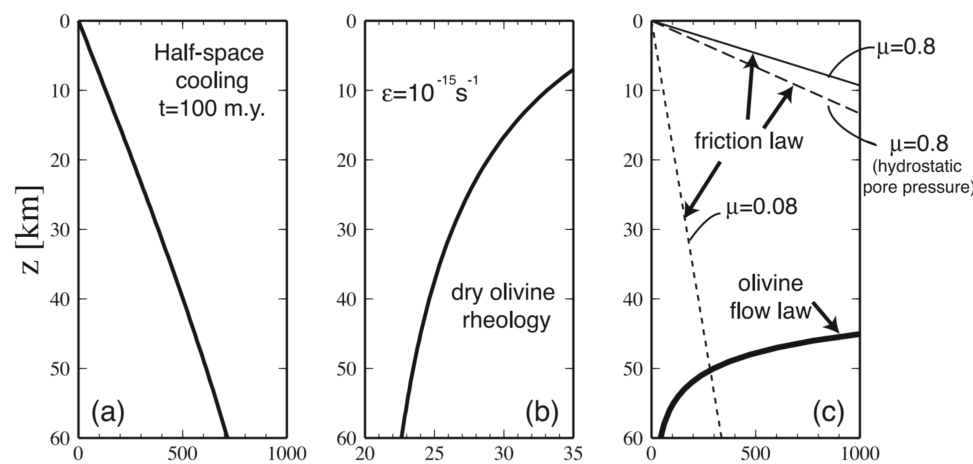

Figure 2. Thermal and rheological structure of oceanic lithosphere 100 Ma after its creation at mid-ocean ridge. (a) Thermal profile according to half-space cooling. (b) Effective viscosity for dislocation creep for dry olivine [*Karato and Jung*, 2003], for the strain rate of 10^{-15} s^{-1}. (c) Corresponding yield stress envelope. Brittle yield stress according to Byerlee's rule is based on optimal thrust faulting [e.g., *Turcotte and Schubert*, 1982] with the friction coefficient of 0.8 (solid) and 0.08 (short-dashed). Effect of hydrostatic pore pressure is also shown (long-dashed).

continental crust contains about 1 wt% H_2O on global average [e.g., *Wedepohl*, 1995], oceanic lithosphere is very dry because of dehydration upon melting as noted earlier. Rehydration by hydrothermal circulation is possible, but its depth extent is not well constrained and is usually believed to be limited to top several kilometers at most [e.g., *Gregory and Taylor*, 1981; *Eiler*, 2001] As recently proposed by *Ranero et al.* [2003], plate bending near a subduction zone may pervasively fault and thus hydrate oceanic lithosphere potentially to substantial depths, but this process could occur only when subduction is already ongoing. What is needed for the self-consistent generation of plate tectonics is, on the other hand, a mechanism to initiate subduction [e.g., *McKenzie*, 1977]. As the history of continental aggregation indicates, the continuous operation of plate tectonics probably demands a mechanism to convert passive margins to active margins [e.g., *Kemp and Stevenson*, 1996; *Regenauer-Lieb et al.*, 2001]; otherwise, the closure of ocean basins would require fairly convoluted tectonics. The Cenozoic history of plate tectonics indicates that the initiation of subduction is likely to have been forced by other ongoing plate tectonic processes, utilizing the preexisting zone of weakness such as spreading ridges and transform faults [e.g., *Gurnis et al.*, 2004; *Schellart et al.*, 2006], but I note that modern geological records are fundamentally biased to the dispersal (as opposed to aggregation) mode of continents. The need of passive margin collapse to close large ocean basins may be debatable, and *Stern* [2004], for example, argues against it on the basis of previous geodynamical studies that suggest that old oceanic lithosphere is too strong to fail [e.g., *Cloetingh et al.*, 1989]. This very notion of strong oceanic lithosphere is, however, what is reassessed in this paper. The closure of the Iapetus (proto-Atlantic) Ocean [e.g., *Wilson*, 1966] is difficult to explain without calling for passive margin collapse, and as far as the spontaneous initiation of subduction is concerned, there is no known mechanism to introduce water into oceanic lithosphere down to the depth of a few tens of kilometers.

[6] The strength of oceanic lithosphere remains as a free parameter, which is varied more or less arbitrarily (with different degrees of sophistication) to create plate tectonic convection in numerical models [e.g., *Gurnis et al.*, 2004; *Stein et al.*, 2004]. As previous studies demonstrated, whether or not plate tectonics could take place is very sensitive to the assigned yield strength; moving from plate tectonics to stagnant lid convection requires a change in maximum yield strength of only 20 MPa in some cases [e.g., *Richards et al.*, 2001]. How to weaken oceanic lithosphere is a key issue in the generation of plate tectonics, because one cannot even discuss other issues such as "plateness" [*Weinstein and Olson*, 1992] and poloidal-toroidal partitioning [*Hager and O'Connell*, 1978] if Earth is trapped in the mode of stagnant lid convection. If low yield strength is required for plate tectonics, it is important to explain how such condition can be achieved by considering tangible physical processes. Going beyond, assuming low yield strength is particularly important if one is interested in deriving the heat flow scaling law of plate tectonics, which plays a critical role in reconstructing the thermal evolution of Earth [e.g., *Conrad and Hager*, 1999; *Korenaga*, 2003, 2006]. The maximum yield strength of oceanic lithosphere may not be a constant in Earth's history, and predicting the yield strength from first principles is essential to investigate the initiation and evolution of plate tectonics.

[7] As a step toward resolving this problem of lithospheric strength, I present a new working hypothesis based on thermal stress accumulation, which has a potential to substantially weaken the otherwise stiffest part of oceanic lithosphere. Thermal stress is caused by elastic response to a change in temperature. The thermoelastic constitutive relation can be expressed as

$$\sigma_{ij} = \delta_{ij}\lambda\varepsilon_{kk} + 2\mu\varepsilon_{ij} - 3\delta_{ij}\alpha_l K\delta T \tag{1}$$

where σ_{ij} and ε_{ij} are stress and strain tensor components, respectively, δ_{ij} is Kronecker's delta, λ and μ are Lamé's elastic constants, α_l is linear thermal expansivity, K is bulk modulus, and δT is temperature difference from some reference temperature, i.e., $\delta T = T - T_0$. The summation convention is assumed for repeated subscripts. The strain tensor is defined in terms of the displacement vector as $\varepsilon_{ij} = (u_{i,j} + u_{j,i})/2$. The last term on the right hand side of equation (1) represents thermal stress. With α_l of 10^{-5}, K of 100 GPa, and temperature drop of 1000 K, thermal stress can be on the order of 1GPa, which is much higher than typical tectonic stress. Of course, viscous relaxation can dissipate this thermal stress, but if lithosphere is so strong due to temperature-dependent viscosity, it may also be able to accumulate enough thermal stress, which could in turn result in fracturing and hydrating the coldest part of oceanic lithosphere. To assess the plausibility of this hypothesis, I conduct the viscoelastic analysis of thermal stress accumulation in cooling oceanic lithosphere. Thermal cracking and its interaction with stress accumulation are also quantified by explicitly modeling the development of tension cracks.

[8] The consideration of thermal stress is not new in marine geophysics. There have been a number of studies on thermal stress in oceanic lithosphere [e.g., *Turcotte and Oxburgh*, 1973; *Parmentier and Haxby*, 1986; *Wessel*, 1992; *Sandwell and Fialko*, 2004], but most of their conclusions appear to be questionable, owing to the use of unlikely physical assumptions, improper boundary conditions, or the crude treatment of mantle rheology. Therefore I begin with presenting a theoretical formulation in some details. Modeling results then follow, based on which previous studies on thermal stress are discussed. Finally, the implications of estimated thermal stress and resultant cracking are explored in terms of the rheological evolution of oceanic lithosphere, together with possible observational tests.

2. Theoretical Formulation

2.1. Governing Equations

[9] A detailed account of viscoelastic thermal stress analysis is available from *Boley and Weiner* [1960], so only a brief summary is given here. First of all, the following momentum balance must always hold:

$$\sigma_{ij,j} + f_i = 0, \tag{2}$$

where f_i denotes the external body force per unit volume. In this study, I set $f_i = 0$, as the focus of this study is on perturbations caused by thermal stress, not on the reference (prestressed) state itself. The effect of gravity appears only in boundary conditions. Noting that only deviatoric stresses are subject to viscous relaxation, the stress and strain tensors are decomposed into the isotropic and deviatoric components as

$$\sigma = \sigma_{ii}/3, \tag{3}$$

$$\varepsilon = \varepsilon_{ii}/3, \tag{4}$$

$$s_{ij} = \sigma_{ij} - \delta_{ij}\sigma, \tag{5}$$

$$e_{ij} = \varepsilon_{ij} - \delta_{ij}\varepsilon. \tag{6}$$

[10] As the isotropic stress-strain relation is always purely elastic, it follows from equation (1) that

$$\sigma = 3K\varepsilon - 3\alpha_l K\delta T. \tag{7}$$

[11] For the deviatoric stress-strain relation, I assume the Maxwell body so that

$$\dot{e}_{ij} = \frac{1}{2\mu}\dot{s}_{ij} + \frac{1}{2\eta}s_{ij}, \tag{8}$$

where the dot denotes (material) differentiation with respect to time and η is viscosity. Using equations (5)–(7), this may be arranged as

$$\dot{\sigma}_{ij} + \frac{\mu}{\eta}\sigma_{ij} = 2\mu\dot{\varepsilon}_{ij} + 3\delta_{ij}\left[\lambda\dot{\varepsilon} - \alpha_l K\delta\dot{T} + K\frac{\mu}{\eta}(\varepsilon - \alpha_l\delta T)\right]. \tag{9}$$

[12] Together with equation (2), this constitutive equation for the Maxwell body forms a foundation for the viscoelastic analysis of thermal stress. For the shallow upper mantle, both λ and μ are assumed to be 60 GPa, which corresponds to Young's modulus of 150 GPa and the Poisson ratio of 0.25. The bulk modulus is then 100 GPa as $K = \lambda + 2\mu/3$. The linear thermal expansivity is one third of volume thermal expansivity, and I adopt the value of 10^{-5} K^{-1}.

[13] The viscosity is evaluated through the following composite rheology model for Earth's mantle:

$$\eta = \sigma_{II}/\left(\dot{e}_f + \dot{e}_s + \dot{e}_p\right). \tag{10}$$

where σ_{II} denotes the second invariant of the deviatoric stress tensor, and $\dot{e}_f$, $\dot{e}_s$, and $\dot{e}_p$ are strain rates for diffusion, dislocation, and Peierls creep mechanisms, respectively. As only the shallowest upper mantle is involved, the influence of the activation volume is neglected here. Flow laws for these creep mechanisms are specified as follows:

[14] Diffusion creep

$$\dot{e}_f = \dot{e}_{f,dry} + \dot{e}_{f,wet}, \tag{11}$$

$$\dot{e}_{f,dry} = A_{f,dry}\sigma_{II}d^{-p}\exp\left(-H_{f,dry}/RT\right), \tag{12}$$

$$\dot{e}_{f,wet} = A_{f,wet}C_{H_2O}^{r_f}\sigma_{II}d^{-p}\exp\left(-H_{f,dry}/RT\right), \tag{13}$$

with $A_{f,dry}$ = 1.58 × 10^9 (s^{-1} MPa μm^p), $A_{f,wet}$ = 10^6 (s^{-1} MPa μm^p), r_f = 1, p = 3, $H_{f,dry}$ = 375 kJ mol^{-1}, and $H_{f,wet}$ = 335 kJ mol^{-1} [*Hirth and Kohlstedt*, 2003]. The water concentration C_{H_2O} is in units of ppm H/Si, the grain size d is in microns, σ_{II} is in MPa, R is the universal gas constant, and T is absolute temperature.

[15] Dislocation creep

$$\dot{e}_s = \dot{e}_{s,dry} + \dot{e}_{s,wet}, \tag{14}$$

$$\dot{e}_{s,dry} = A_{s,dry}\sigma_{II}^n\exp\left(-H_{s,dry}/RT\right), \tag{15}$$

$$\dot{e}_{s,wet} = A_{s,wet}C_{H_2O}^{r_s}\sigma_{II}^n\exp\left(-H_{s,wet}/RT\right), \tag{16}$$

with $A_{s,dry}$ = 1.26 × 10^6 (s^{-1} MPa^{-n}), $A_{s,wet}$ = 3.63 (s^{-1} MPa^{-n}), r_s = 1.2, n = 3, $H_{s,dry}$ = 510 kJ mol^{-1}, and $H_{s,wet}$ = 410 kJ mol^{-1} [*Karato and Jung*, 2003].

[16] Peierls creep

$$\dot{e}_p = A_p\exp\left[-\frac{H_p}{RT}\left(1 - \frac{\sigma_{II}}{\sigma_P}\right)^2\right], \tag{17}$$

with A_p = 5.7 × 10^{11} s^{-1}, H_p = 536 kJ mol^{-1}, and σ_P = 8.5 × 10^3 MPa [*Goetze and Evans*, 1979]. Note that this formula is valid only when σ_{II} >200 MPa. For stresses below this threshold, $\dot{e}_p$ is set to zero.

[17] For the evolution of the temperature field, half-space cooling [e.g., *Carslaw and Jaeger*, 1959, p. 59] is adopted:

$$T^{\mathrm{HSC}}(t,z) = T_s + (T_0 - T_s)\,\mathrm{erf}\left(\frac{z}{2\sqrt{\kappa t}}\right), \tag{18}$$

where T_s is the surface temperature (273 K), T_0 is initial mantle temperature (1573 K), κ is thermal diffusivity (10^{-6} m^2 s^{-1}), t is time, and z is a vertical coordinate originated at the surface.

2.2. Model Geometries and Boundary Conditions

[18] Two complementary plane strain models are considered: ridge-parallel cross section (Figure 3, case A) and ridge-normal cross section (Figure 3, case B). The ridge-parallel model aims to track the temporal evolution of thermal stress, with or without crack growth. On the other hand, the ridge-normal model is designed to obtain a quasi-steady state solution for thermal stress distribution in the case of no crack growth. My emphasis is on the ridge-parallel model because, as suggested later by the ridge-normal model, the results of the ridge-parallel model are probably applicable to ridge-normal crack growth as well. As these models are two-dimensional, only very simple planforms of crack formation can be treated.

[19] The ridge-parallel model assumes the one-dimensional temperature field of half-space cooling, $T(t, z)$, at any given time (equation (18)). The top boundary is free surface, and the vertical displacement and the horizontal traction are set to zero at the bottom. The horizontal displacement and the vertical traction are set to zero at the left boundary. In case of no crack growth, the right boundary shares the same boundary conditions with the left

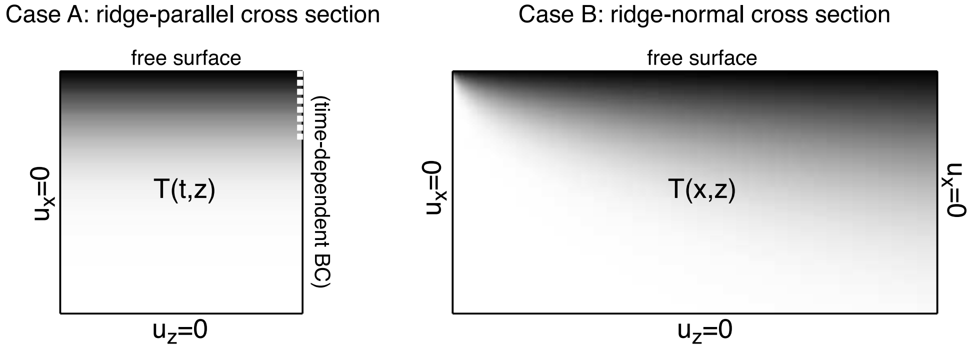

Figure 3. Two model geometries used in this study. In ridge-parallel models, temperature is one-dimensional but time-dependent. The boundary condition on the right boundary is time-dependent when simulating crack growth. In ridge-normal models, temperature is two-dimensional, and its installment is either instantaneous or gradual. See text for details.

boundary. Stress and displacement are calculated assuming purely elastic response (i.e., equation (1)) at $t = 0$, and the subsequent temporal evolution is modeled by integrating equation (9).

[20] The presence of a crack is modeled by unconstraining both horizontal and vertical displacements for some top fraction of the right boundary (e.g., dashed white line in Figure 3) and also by specifying appropriate boundary traction. Both the left and right boundaries are the line of symmetry, and this model is limited to equally spaced cracks; to model cracks with a regular spacing of 100 km, for example, the horizontal extent of the model has to be only 50 km. The horizontal traction on the crack wall is given by

$$\sigma_{xx}|_{x=x_{\max}} = (\rho_m - \rho_w)gz, \tag{19}$$

where ρ_m is mantle density (3300 kg m^{-3}), ρ_w is water density (1000 kg m^{-3}), and g is gravitational acceleration (9.8 m s^{-2}). Because gravity is not considered in the equilibrium equation (equation (2)) and because crack space in oceanic lithosphere is supposed to be filled with water, the horizontal traction is equal to the difference between lithostatic and hydrostatic pressures. The vertical traction on the crack wall is zero, as water does not support shear stress.

[21] Crack growth is simulated by changing the length of the unconstrained boundary according to a change in the stress field. In fracture mechanics, the condition for crack growth is usually discussed in terms of the stress intensity factor or the J integral because of stress singularity at a crack tip [e.g., *Lawn and Wilshaw*, 1975; *Anderson*, 2005]. Instead of accurately calculating the stress intensity factor for a given crack, the following simplified procedure is used for crack growth: a crack is extended so that stress beneath the crack tip is always lower than the confining pressure, $(\rho_m - \rho_w)\, gz$. This approximated procedure is motivated by the work of *Lachenbruch* [1961], who studied the fracture mechanics of tension cracks with the effect of gravity. He showed that the crack growth is controlled by the following balance in the stress intensity factor:

$$K_\Theta + K_\rho = K_c, \tag{20}$$

where K_Θ and K_ρ are the stress intensity factors due to thermal stress and confining pressure, respectively, and K_c is fracture toughness of material under consideration. For lithospheric-scale cracks (i.e., longer than a few kilometers), K_Θ and K_ρ are both on the order of a few GPa m$^{1/2}$ with opposite signs (K_ρ is negative because confining pressure tries to close cracks). On the other hand, the fracture toughness of polycrystalline olivine is known to be around 1 MPa m$^{1/2}$ [*deMartin et al.*, 2004]. Thus, for the growth of lithospheric-scale crack, the right-hand side of equation (20) is effectively zero, and crack growth is controlled by the balance between thermal stress and confining pressure.

[22] Crack growth modifies the stress and displacement fields as follows:

$$\sigma_{ij}|_{t=t_c^+} = \sigma_{ij}|_{t=t_c^-} + \Delta\sigma_{ij} \tag{21}$$

$$u_{ij}|_{t=t_c^+} = u_{ij}|_{t=t_c^-} + \Delta u_{ij} \tag{22}$$

where t_c^+ and t_c^- denotes times just after and before a crack extends incrementally from some depth of z_o to $z_n (> z_o)$. As this incremental crack growth takes place instantaneously (at least in a geological sense), viscous relaxation is likely to be unimportant, and the above changes in stress and displacement may be calculated by using the principle of superposition in linear elasticity [e.g., *Anderson*, 2005]. At $t = t_c^-$, the uncracked segment from z_o to z_n can be regarded as cracked but closed by a hypothetical traction equal to thermal stress. At $t = t_c^+$, this segment is cracked and open and subject to the confining pressure. As there is no change in the temperature field during this instantaneous crack growth, therefore $\Delta\sigma_{ij}$ and $\Delta\ u_{ij}$ can be calculated as the elastic response of a thermally homogeneous medium to the following traction on the newly created crack segment:

$$\sigma_{xx}|_{x=x_{\max},\, z_o<z<z_n} = -\sigma_{xx}|_{x=x_{\max},\, z_o<z<z_n,\, t=t_c^-} + (\rho_m - \rho_w)gz. \tag{23}$$

For this calculation, traction on other parts of the boundary is zero, and displacement boundary conditions are the same as previously described.

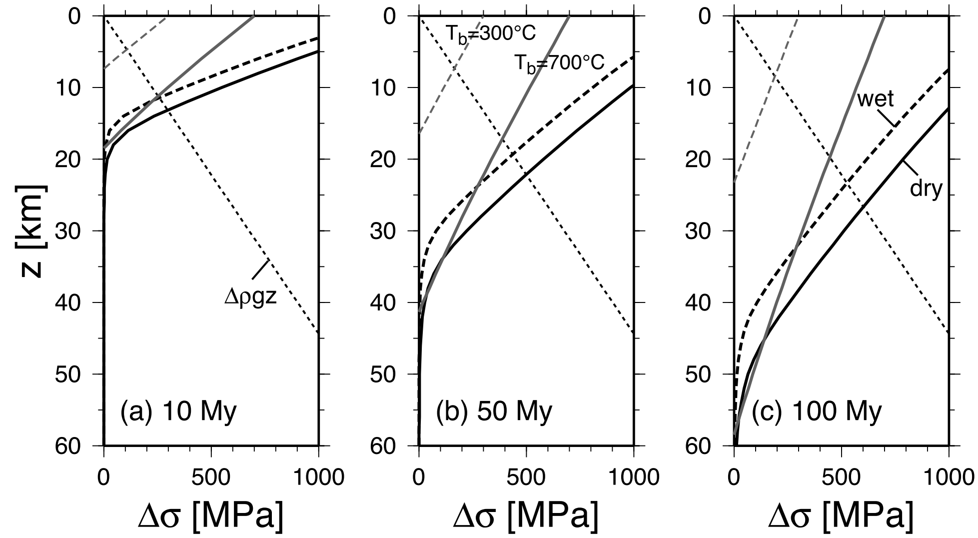

Figure 4. Ridge-parallel model with no crack growth. Snapshot of differential stress, $\Delta\ \sigma(=\sigma_{xx})$, at (a) t = 10 Ma, (b) t = 50 Ma, and (c) t = 100 Ma. Two cases for dry mantle (solid) and wet mantle (dashed) are shown, together with the elastic approximation with the blocking temperature (300°C (gray dashed) and 700°C (gray)). Confining pressure is also shown for comparison (dotted).

[23] The ridge-normal model also assumes half-space cooling, but in this case, the temperature field is two-dimensional because of horizontal plate velocity U (Figure 3). As shown in section 3, my numerical scheme is formulated in the framework of compressible elasticity. The steady state distribution of thermal stress in the moving thermal boundary layer cannot be modeled properly in this framework. For the sake of discussion, however, we may still benefit from some exploratory models, which mimic this steady state cross section in an approximated way. To this end, I model the evolution of thermal stress in a static viscoelastic medium with a prescribed two-dimensional temperature field. Two ad hoc different temperature fields are tested: (1) the frozen mode in which temperature is time-independent as $T(x, z, t) = T^{\mathrm{HSC}}(x/U, z)$, and (2) the gradual mode with $T(x, z, t) = T^{rmHSC}(xt/(Ut_{\max}), z)$, where $t_{\max}$ controls the rate of temperature evolution.

[24] As in the ridge-parallel model, the top boundary is free surface, and the bottom has zero vertical displacement and free slip. The left and right boundaries have zero horizontal displacement and free slip. While the left boundary (i.e., just beneath a spreading center) must have zero horizontal displacement because it is the line of symmetry (note that oceanic crust is neglected in this study, so is its accretion at a ridge axis), there is no reason to impose zero horizontal displacement on the right boundary. The entire plate may be in extension or compression depending on tectonic situations. In this regard, my model should be considered as a tectonically neutral case. A primary goal here is to investigate how horizontal temperature gradient may affect thermal stress accumulation in a viscoelastic medium, and this model will prove to be sufficient for discussion.

3. Results

[25] The finite element method is employed to obtain numerical solutions for the initial value problems as defined above. The derivation of matrix equations for these viscoelastic problems is given in Appendix A.

3.1. Ridge-Parallel Models

[26] The simplest ridge-parallel model is the one without any crack growth, in which the horizontal displacement is suppressed by having fixed vertical boundaries. I used 100 × 1 uniform elements to model this essentially one-dimensional case with the depth extent of 100 km. For mantle rheology, two water contents are tested: 10 ppm H/Si (dry) and 1000 ppm H/Si (wet). The latter is believed to be appropriate for asthenosphere. Fractional melting brings down water content far below 10 ppm H/Si [e.g., *Hirth and Kohlstedt*, 1996], but using a lower water content does not result in stiffer lithosphere because water-independent creep mechanisms (e.g., equation (12)) place the upper limit on effective viscosity. Grain size is assumed to be 5 mm [*Ave Lallemant et al.*, 1980] for all of my calculations.

[27] The result of this model calculation for 100 Ma is shown in Figure 4. The maximum thermal stress easily exceeds 1 GPa all the time, and at 100 Ma, the top 40–50 km of oceanic lithosphere accumulates thermal stress greater than 100 MPa. Though I use the composite rheology model incorporating diffusion, dislocation, and Peierls creep mechanisms, the dominant deformation mechanism turns to be usually diffusion creep. This is expected because diffusion creep has the lowest activation energy. Dislocation creep could be more efficient when stress is high, but high thermal stress is always associated with low temperature. Thus, even in the high stress regime, diffusion creep is most efficient. The Peierls mechanism is never activated simply because stress involved is just too low for this mechanism to be dominant.

[28] Note that all of flow laws used in the composite rheology model are for steady state deformation. Total strain involved in thermal contraction is, on the other hand, too small to be considered with steady state flow laws, and it

should be treated with transient flow laws. Because of the paucity of experimental data, however, the transient creep of mantle olivine is not well understood in contrast to its steady state deformation. On the basis of theoretical consideration combined with available data, *Karato* [1998] estimated that effective viscosity for transient creep could be lower than that for steady state creep by up to an order of magnitude, because only soft slip systems have to be invoked to accommodate small strain. This possible softening by transient creep is probably not very important for the present thermoelastic analysis, however. As can be seen in Figure 4, the dry and wet cases result in similar thermal stress profiles, with only ~5 km difference at most regarding the depth extent. The water contents assumed for these two cases are different by two orders of magnitude, and thus a similar difference is expected for effective viscosity (equations (13) and (16)). Thermal stress accumulation in dry lithosphere with more realistic transient creep is therefore likely to be bounded by these two similar profiles. In the following, only dry lithosphere is considered (i.e., $C_{\mathrm{H_2O}}$ = 10 ppm H/Si).

[29] In most of previous studies on thermal stress in oceanic lithosphere, the viscoelastic accumulation of thermal stress is approximately handled by an elastic model with the so-called blocking temperature [e.g., *Turcotte*, 1974; *Parmentier and Haxby*, 1986; *Sandwell*, 1986]. That is, thermal stress is assumed to accumulate only after temperature falls below the blocking temperature, T_b:

$$\Delta\sigma_{ij}^{T} = \begin{cases} -3\delta_{ij}\alpha_l K(T - T_b) & \text{if } T < T_b \\ 0 & \text{otherwise.} \end{cases} \tag{24}$$

[30] *Turcotte* [1974] adopted T_b = 300°C, and later studies tend to use higher values. The thermal stress accumulation based on this approximation is also shown in Figure 4 for T_b = 300°C and 700°C. It can be clearly seen that T_b = 300°C grossly underestimates the magnitude of thermal stress, and also that the use of the blocking temperature, regardless of its magnitude, fails to reproduce the depth gradient of thermal stress.

[31] The extremely high thermal stress seen at shallow depths would not be achieved in reality, because it is well above the brittle strength of the mantle. Crack growth has to be incorporated in order to make model predictions more realistic. The crack spacing of 200 km is considered first. As will be shown, this spacing is so wide that the model is effectively about the growth of a single crack in a horizontally infinite medium. Utilizing the model symmetry (Figure 3), the finite element model is 100 km wide and 100 km deep, with the grid interval of 1 km both horizontally and vertically. The model is sufficiently deep so that results are insensitive to the boundary condition at the base. Modeling results indicate that thermal cracking could fracture lithosphere fairly deeply, reaching the depth of ~10, ~20, and ~30 km at t = 10, 50, and 100 Ma (Figure 5). It is also noted that the crack formation releases thermal stress only locally, with the horizontal extent of stress release being nearly proportional to crack depth. The region away from this crack still suffers from thermal stress exceeding fracture strength, so more narrowly spaced cracks are considered next.

[32] The second crack model has 30-km spacing (Figure 6). Cracks grow in a manner very similar to the first model, with the crack depth being slightly shallower. As expected, stress release is more pervasive. Because deep cracks do not release stress at shallow depths very efficiently, however, there are still shallow regions with high thermal stress. These regions must be fractured by more narrowly spaced shallower cracks, and the cascade crack structure would be ideal in terms of stress release. I note, however, even with this ideal crack system, thermal stress cannot be completely removed. First of all, thermal stress below crack depth is almost unchanged by crack formation (Figures 5 and 6), and this deep thermal stress is still of a significant magnitude (a few hundred megapascals). Second, as far as crack space is connected to overlying seawater, crack walls are always subject to the confining pressure, $(\rho_m - \rho_w)\, gz$, so thermal stress cannot fall below this pressure. The lowest thermal stress that could be achieved by the ideal crack system is therefore zero at the surface, increasing linearly following the confining pressure down to some depth (e.g., ~30 km for t = 100 Ma), and then decreasing almost linearly to a midlithospheric depth.

[33] The above model is only applicable to crack formation perpendicular to a ridge axis. The evolution of cracks with a different orientation may be different from this, because lateral variations in temperature, which are absent from the ridge-parallel model, may affect the evolution of thermal stress considerably. In order to evaluate this effect of lateral variations, the ridge-normal geometry is considered next.

3.2. Ridge-Normal Models

[34] As described in section 2.2, two different temperature fields, the frozen and gradual modes for this model geometry, are used. The spreading rate is set to 2 cm yr^{-1}, and I test two different horizontal extents, 1000 km and 2000 km, which correspond to 50 Ma and 100 Ma, respectively. The model domain is discretized with uniform elements, each of which is 40-km-wide and 2-km-high. Selected model results are shown in Figure 7. How to set up the temperature field has a significant effect on thermal stress, as can be seen from Figures 7a and 7b. The frozen mode, in which the thermal boundary layer is instantaneously introduced, leads to excessively high thermal stress in lithosphere (Figure 7a). This is clearly unrealistic because viscous relaxation during the growth of the boundary layer is not considered at all in this instantaneous setup. The magnitude of thermal stress in the gradual mode (Figure 7b) is similar to what is obtained in the ridge-parallel model. This static model can only be a crude approximation to the true steady state, and the gradual mode appears to be sufficient for us to gain some quantitative understanding of the ridge-normal structure. By comparing the frozen-mode models with different widths (Figures 7b and 7c), the right boundary seems to have little effect on the overall structure of thermal stress.

[35] Figure 7d shows another attempt to emulate the steady state thermal stress based on the ridge-parallel model. I simply convert the temporal progression of ridge-parallel thermal stress (as shown in Figure 4) to the spatial distribution of ridge-normal thermal stress by translating time to distance using the spreading rate. The gradual

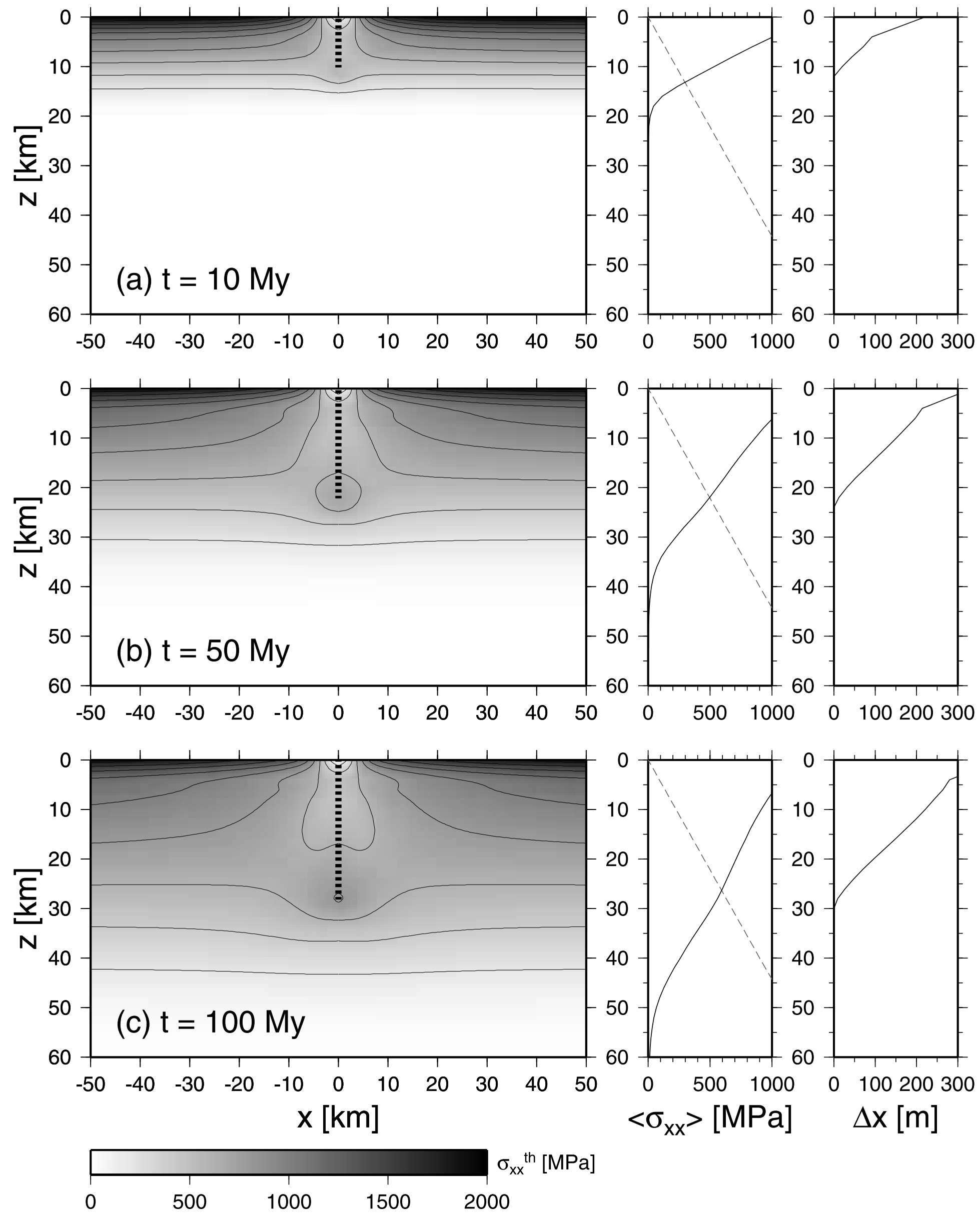

Figure 5. Ridge-parallel model with 200-km crack spacing. The actual model domain spans from −100 km to 0 km in the horizontal coordinate and from 0 km to 100 km in the vertical coordinate. The release of thermal stress due to crack formation is limited with horizontal extent similar to crack depth, and this model can be regarded as single crack formation in a horizontally infinite medium. (left) Horizontal thermal stress, (middle) its horizontal average (confining pressure as dashed line), and (right) crack opening. In Figure 5 (left), the depth extent of crack is indicated by thick dotted line, and the contour interval is 200 MPa.

mode model differs from this ridge-parallel-based model up to a few hundred megapascals (Figure 7e), but these two models are still very similar in the depth extent of finite thermal stress (e.g., >40 km deep at 100 Ma), and the maximum thermal stress is greater than 1 GPa in both models at any given time. These similarities suggest that the thermal stress evolution in the ridge-normal cross section may well be approximated by that in the ridge-parallel cross section. In other words, the horizontal temperature gradient in the ridge normal direction could safely be neglected when considering thermal stress at regional scales. This may be obvious from the vertical exaggeration used in Figure 7. The horizontal temperature gradient is even smaller for higher spreading rates.

[36] In all of the ridge-normal models, stresses are virtually zero along the left boundary, because hot and thus low-viscosity mantle beneath the ridge axis can dissipate thermal stress quickly (i.e., less than a few thousand years). Note that I did not impose this zero horizontal traction beneath the ridge axis as a boundary condition. Though zero horizontal traction (i.e., free-moving boundary) has often been used for the ridge axis in the past [e.g., *Haxby and Parmentier*, 1988], the left boundary must have zero horizontal displacement, as it is required by symmetry. This is

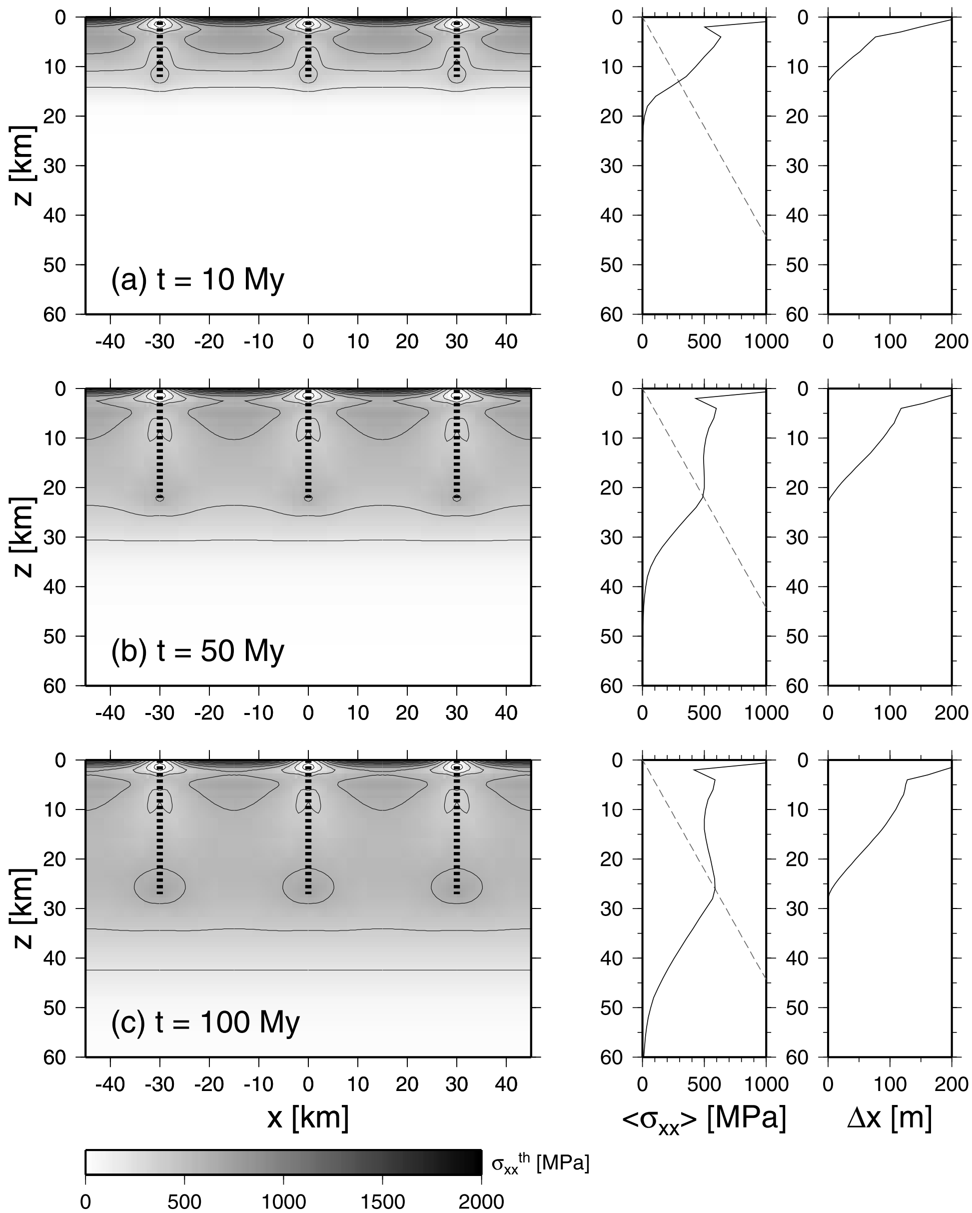

Figure 6. Same as Figure 5, but with 30-km crack spacing. The model domain spans only from −15 km to 0 km in the horizontal coordinate, and the solution is simply repeated at the vertical lines of symmetry for plotting purpose.

true not only for my static model, but also for the real steady state situation. Zero horizontal traction should emerge naturally from viscous relaxation and should not be imposed as a boundary condition. When the elastic approximation with the blocking temperature was used in previous studies, this point was usually not appreciated.

4. Discussion

4.1. Critique of Previous Studies on Thermal Stress

[37] As noted in Introduction, the consideration of thermal stress in evolving oceanic lithosphere is not new. After *Turcotte and Oxburgh* [1973] indicated the potential importance of thermal stress in lithospheric dynamics, thermal stress has been studied to explain the spacing of transform faults [*Turcotte*, 1974; *Sandwell*, 1986], to model the ambient stress state [*Bratt et al.*, 1985; *Haxby and Parmentier*, 1988; *Denlinger and Savage*, 1989] as well as the temporal evolution of fracture zones [*Parmentier and Haxby*, 1986; *Wessel and Haxby*, 1990], and to evaluate its role in elastic thickness estimates based on lithospheric flexure [*Wessel*, 1992]. An interest in thermal stress has been recently revived as a potential mechanism to explain the origin of gravity rolls in the southern Pacific [*Gans et al.*, 2003; *Sandwell and Fialko*, 2004].

[38] Beyond the order of magnitude argument by *Turcotte and Oxburgh* [1973], however, all of previous attempts to model thermal stress more quantitatively are at odds with the present study. To simplify discussion, I will focus on the

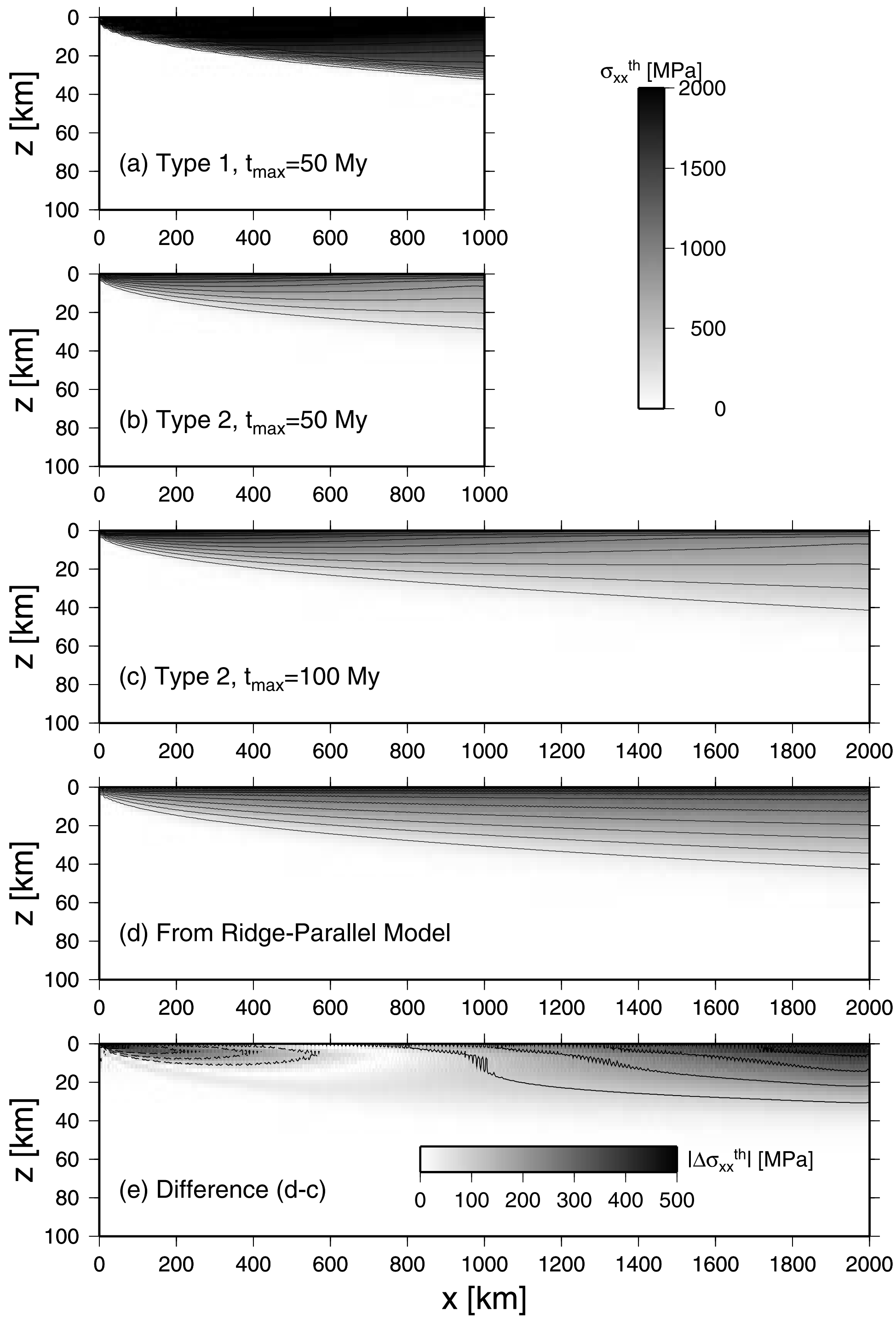

Figure 7. Various attempts to model steady state ridge-normal cross section. Spreading rate is set as 2 cm yr^{-1} for all models. The 1000-km-long ridge-normal models are shown with (a) frozen mode temperature and (b) gradual mode temperature; (c) 2000-km-long model with gradual mode temperature; (d) inference based on the ridge-parallel model; (e) the difference between the above two models.

ridge-parallel cross section. On the basis of the modeling results given in section 3.2, my reasoning could possibly be extended to the ridge-normal cross section as well, but this remains speculative at this point. The most obvious discrepancy between this study and previous ones is in the sense of horizontal thermal stress; it is always tensional everywhere in my models (e.g., Figure 6), whereas it is compressional at shallow depths and tensional at greater depths in previous studies [e.g., *Turcotte*, 1974; *Parmentier and Haxby*, 1986; *Wessel*, 1992]. To understand the cause of this discrepancy, there are three important issues to be discussed: (1) the treatment of viscoelasticity, (2) boundary conditions, and (3) the applicability of Saint-Venant's principle.

[39] First, in most of previous studies, viscoelastic thermal stress has been modeled approximately using the thermoelastic theory modified with the blocking temperature (equation (24)). Though Figure 4 may indicate that this simplified approach is reasonable as far as the blocking temperature is appropriately chosen (e.g., 700°C), this elastic approach has a hidden pitfall, which will become apparent when I discuss Saint-Venant's principle later. Notable exceptions to this blocking temperature approach are the use of the stress relaxation timescale by *Bratt et al.* [1985] and the fully viscoelastic approach by *Denlinger and Savage* [1989]. *Bratt et al.* [1985], however, assumed at the outset that thermal stress is relieved on time scales short compared to the age of lithosphere (and independent of the viscosity structure of lithosphere), and went on to adopt a fairly ad hoc method of thermal stress calculation, which is impossible to justify. *Denlinger and Savage* [1989] has been the only study that used viscoelasticity, but mantle viscosity assumed in their study is too low. They tested two diffusion creep models, and while the activation energy is reasonable in both models ($\sim$300–400 kJ mol^{-1}), reference viscosity at 1300°C is 10^{19} Pa s for one model and $10^{11.75}$ Pa s for the other model. The former is now generally regarded as the viscosity of asthenosphere and not of dry depleted lithosphere, which is believed to be more viscous by 2 orders of magnitude. The latter is unbelievably low. *Denlinger and Savage* [1989] cited *Karato et al.* [1986] for this viscosity, but this viscosity corresponds to that of fine-grained olivine aggregates used in laboratory experiments and should not be used for Earth's mantle, in which the grain size of olivine is on the order of millimeters, not microns.

[40] Second, previous models assumed free traction at the vertical boundaries (e.g., fracture zones in the ridge-parallel cross section). Even if fracture zones are completely fractured to great depths, however, horizontal traction cannot be zero at those boundaries because the difference between lithostatic and hydrostatic pressures would always exert tensional traction. In the presence of this confining pressure, one has to invoke some additional mechanism to achieve free traction at vertical boundaries.

[41] Finally, even if boundary traction somehow vanishes, this zero traction does not lead to compressional stress at shallow depths and extensional stress at greater depths, contrary to a common belief in previous studies. A conventional argument is all based on the following assumption: for a freely deforming plate, thermal stresses averaged over its thickness D are always zero, e.g.,

$$\int_0^D \sigma_{xx}(x,z)dz = 0. \tag{25}$$

[42] Though this might appeal to intuition, one cannot derive this from the conservation of momentum alone. In the absence of external force, two-dimensional momentum balance relevant to σ_{xx} is the following:

$$\frac{\partial \sigma_{xx}(x,z)}{\partial x} + \frac{\partial \sigma_{xz}(x,z)}{\partial z} = 0. \tag{26}$$

[43] By integrating this with respect to z, one may obtain

$$\frac{\partial}{\partial x}\int_0^D \sigma_{xx}(x,z)dz + [\sigma_{xz}(x,z)]_0^D = C(x), \tag{27}$$

where $C(x)$ is an arbitrary function of x only. When the horizontal boundaries are free slip, the second term on the left-hand side is zero. By one more integration and applying zero horizontal traction at $x = 0$, we may arrive at:

$$\int_0^D \sigma_{xx}(x,z)dz = \int_0^x C(x')dx'. \tag{28}$$

[44] Thus equation (25) does not hold in general, and it requires additional assumptions for the right-hand side to be zero. Equation (25) is known to be a good approximation for a thin elastic plate (i.e., $x \gg D$), and this is sometimes loosely referred to as the application of Saint-Venant's principle [e.g., *Boley and Weiner*, 1960, p. 278] (for a more precise description of this principle, see *Fung* [1965]). Saint-Venant's principle is usually expected to work well for simple elastic bodies, and it might also work even with yielding [e.g., *Fung*, 1965, p. 307]. Its general applicability to viscoelastic bodies, however, is not expected, and as I will demonstrate shortly, Saint-Venant's principle works only under limited conditions.

[45] Figure 8 illustrates how the use of equation (25), when combined with the notion of the blocking temperature, leads to compressional stress at shallow depths. As cooling proceeds, the depth at which cooling is most efficient (i.e., dT/dt is at its maximum) gradually increases (Figure 8b). Only the cooling below the blocking temperature contributes to thermal stress. Because the vertically averaged thermal stress must be zero, the "effective" temperature increment is positive at shallow depths and negative at greater depths (Figure 8c). The resulting thermal stress therefore becomes compressional at shallow depths and extensional at greater depths, as shown in Figure 8d. This state of stress in oceanic lithosphere is a prevailing notion in existing literature, and there are at least two reasons I can imagine why this is so. First of all, this stress state appears to be nicely consistent with the observed pattern of focal mechanisms in young oceanic lithosphere [*Bergman and Solomon*, 1984; *Wiens and Stein*, 1984], and this observation is frequently mentioned in previous studies as circumstantial evidence [e.g., *Parmentier and Haxby*, 1986; *Haxby and Parmentier*, 1988; *Denlinger and Savage*, 1989; *Wessel*, 1992]. Second, this type of stress state has also been known to exist in thermally tempered glass [e.g., *Lee et al.*, 1965; *Narayanaswamy and Gardon*, 1969]; compressional stress near glass surface is what increases the strength of glass. As the viscosity of glass materials is temperature-dependent as strongly as that of mantle materials, this small-scale analogue may appear to be conflicting with my numerical results.

[46] There are, however, important differences between glass tempering and the thermal evolution of oceanic lithosphere, and these differences happen to matter for the resulting state of thermal stress. In thermal tempering processes, glass is cooled from both surfaces and surface temperature is lowered gradually (by natural or forced air

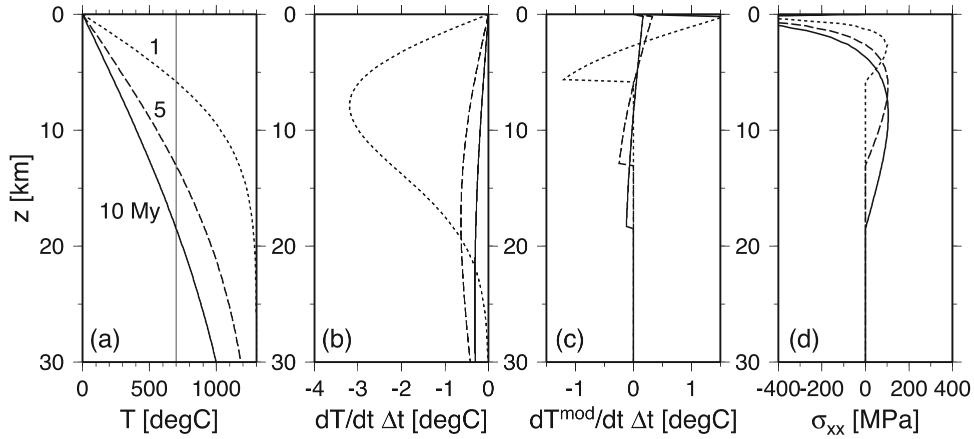

Figure 8. How previous studies have modeled the ambient stress state of oceanic lithosphere [e.g., *Parmentier and Haxby*, 1986; *Haxby and Parmentier*, 1988; *Wessel*, 1992]. (a) Geotherms at t = 1 (dotted), 5 (dashed), and 10 Ma (solid). The blocking temperature of 700°C is also shown for reference. (b) Corresponding cooling rate, with Δt of 0.01 Ma. (c) Modified cooling rate constructed by first removing the contribution above the blocking temperature and then removing the vertical average. (d) Corresponding horizontal thermal stress at t = 1 (dotted), 5 (dashed), and 10 Ma (solid). It is compressional at shallow depths and tensional at greater depths.

convection), not instantaneously [e.g., *Gardon*, 1980]. This doubled-sided gradual cooling is essential to avoid breakage during tempering, by preventing a large temperature contrast to develop in glass. This is very different from the half-space cooling of oceanic mantle, in which surface temperature is set to zero instantaneously at t = 0 and the cooling of the interior is much less efficient than double-sided cooling. In half-space cooling, therefore tensional stress near the cold surface is more likely to be frozen in and hard to be affected by the subsequent (minor) accumulation of thermal stress in greater depths.

[47] To demonstrate my point, I ran the ridge-parallel model with free traction on the right boundary, using both instantaneous cooling and double-sided gradual cooling (Figure 9). In the gradual cooling, top and bottom temperature are lowered, linearly from 1300°C to 0°C, over the first 50 Ma. In addition to the composite mantle rheology model, simple temperature-dependent viscosity is also tested with the activation energy of 300 kJ mol^{-1} and the reference value of 10^{21} Pa s at 1300°C. Double-sided gradual cooling, regardless of viscosity models, results in compressional stress near surfaces and extensional in the middle (Figure 9f), which is very similar to what is observed for tempered glass. For instantaneous half-space cooling, however, results depend greatly on the choice of a viscosity model, and more importantly, equation (25) does not hold. It appears that the half-space cooling results in too large a viscosity contrast for Saint-Venant's principle to work. Compared to the simple temperature-dependent viscosity model, the composite rheology model gives a lower viscosity contrast, so the corresponding thermal stress is less tensional (Figures 9a–9c), but it is still far from what is commonly believed (Figure 8). When a viscoelastic problem is approximated as an elastic problem with the blocking temperature, one may be tempted to think only in the framework of elastic theory. Saint-Venant's principle is valid only for elasticity, and we should not use it for a fundamentally viscoelastic problem. This is the aforementioned hidden pitfall for the use of the blocking temperature.

[48] Thus it is probably fair to suggest that previous inferences on the state of the thermal stress in oceanic lithosphere are misleading because (1) zero traction at fracture zones is difficult to achieve in the presence of gravity, and (2) even if zero traction is achieved, vertically averaged thermal stresses are not zero for mantle rheology and instantaneous cooling. This implies that what has been explained by thermal stress, such as the pattern of focal mechanisms and fracture zone flexure, may need to be revisited.

4.2. Rheological Evolution of Oceanic Lithosphere

[49] The depth extent of thermal cracking predicted by my modeling is significant (Figure 6); 100 Ma-old lithosphere can be cracked down to ~30 km depth, and thermal stress is greater than confining pressure to keep the crack space open, or more precisely, filled with water. It is important not to confuse this large-scale thermal crack with microcracks. Microcracks cannot remain open at such great depths because of confining pressure. As speculated in section 3.1, the most likely crack system would have a cascade structure, composed of widely spaced (~30-km interval) deep cracks and more narrowly spaced shallow cracks. Other crack structures, such as narrowly spaced deep cracks, may be possible, but they do not lead to any additional release of thermal stress.

[50] I also note that stress release by thermal cracking is local. Transform faults or fracture zones alone cannot release thermal stress efficiently. The spacing of transform faults vary from ~30 km to ~1000 km in the global mid-ocean ridge system, with the average of ~160 km [*Sandwell*, 1986]. Thus transform faults and fracture zones are usually too widely spaced, and thermal stress in-between should be strong enough to generate another deep cracking.

[51] Even with the cascade crack system, residual thermal stress is still substantial within the upper half of lithosphere

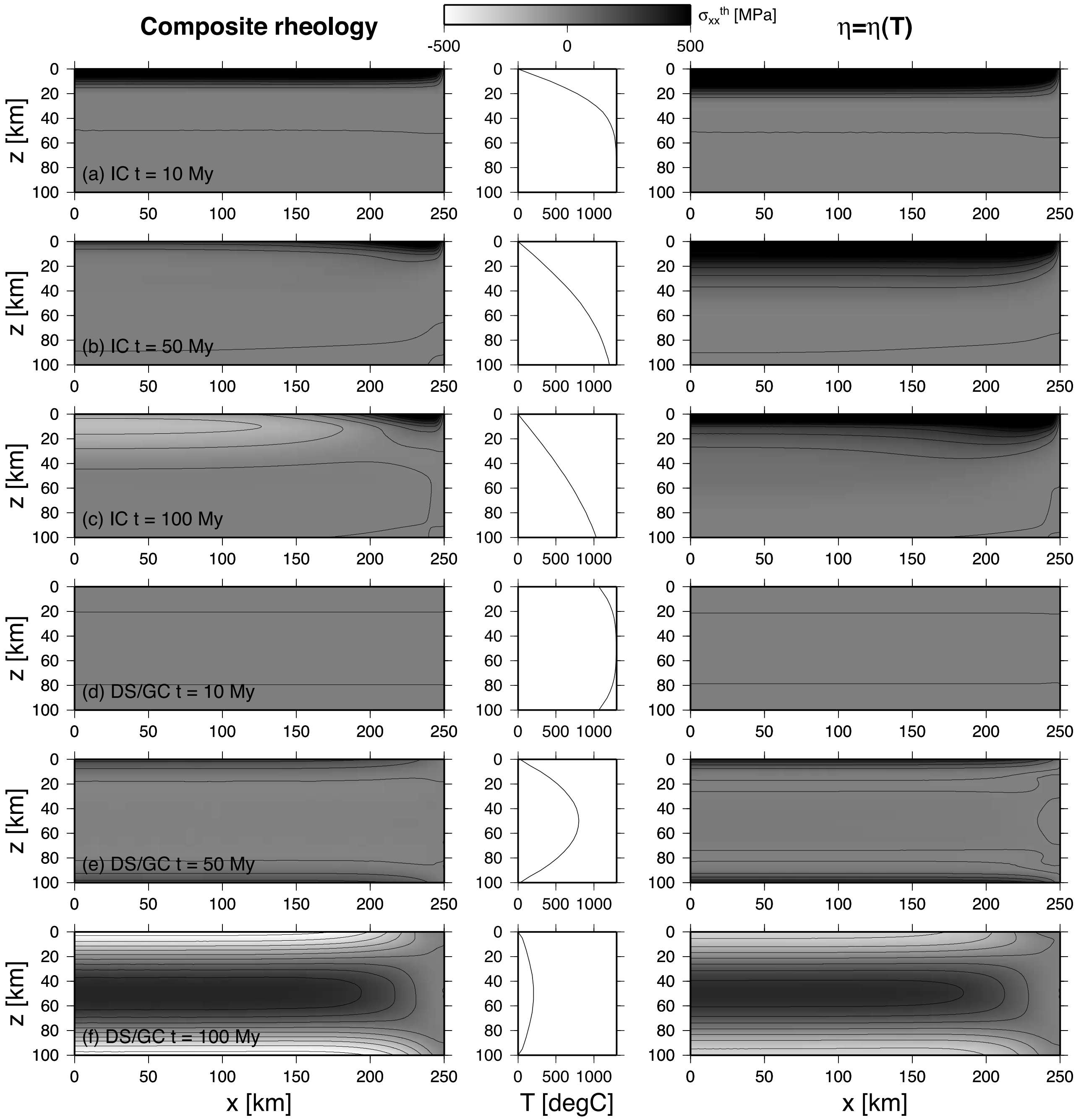

Figure 9. Ridge-parallel models with the free-moving right boundary (i.e., displacement is totally unconstrained). (right) With the composite mantle rheology model, and (left) with simpler, temperature-dependent viscosity with the activation energy of 300 kJ mol^{-1} and the reference viscosity of 10^{21} Pa s. In Figures 9 (left) and 9 (right), horizontal thermal stress is shown with a contour interval of 100 MPa. (middle) Temperature profile. (a–c) Instantaneous half-space cooling and (d–f) double-sided gradual cooling at t = 10, 50, and 100 Ma. The model domain is 250 km wide and 100 km deep. The model width is chosen to show the horizontal extent of edge effects. See text for discussion.

(Figure 10). This residual stress is tensional and on the order of a few hundred megapascals This would be the ambient state of stress in oceanic lithosphere if no process other than cracking takes place. In the presence of surface water, however, this is unlikely. Thermal cracking introduces seawater deeply into cold lithospheric mantle, and the temperature and pressure conditions are ideal for serpentinization. One may expect that volume expansion associated with serpentinization may close the crack space, but this is dynamically not feasible for the following reason. Crack opening is about 100 m (Figure 6), and to consume water in this crack space by serpentinization, this water must be physically transported horizontally into the crack walls. This horizontal water transport has to compete with full

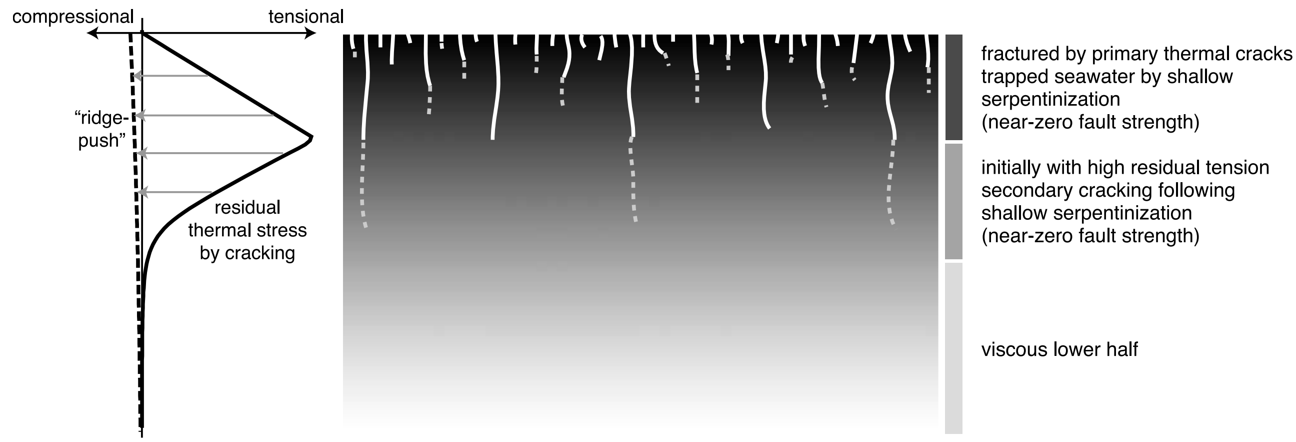

Figure 10. Conceptual drawing for the rheological evolution of oceanic lithosphere. Residual thermal stress after optimal stress release by cascade crack system is shown on the left, together with compressional stress due to "ridge push." In addition to thermal cracking, some mechanism, such as partial crack healing by shallow serpentinization, must exist to liberate this large tensional residual stress, in order to bring oceanic lithosphere in a compressional stress state.

lithostatic pressure, because, unlike the horizontal component, the vertical component of thermal stress is completely released by free-moving seafloor. Although serpentinization is chemically favored, therefore it is unlikely to consume all water in the crack space except at very shallow depths. Of course, one must consider more complicating factors in the real world, because the crack space would not be occupied not only by seawater but also by sediment infill and debris from crack walls. The possibility of chemical reaction being regulated by the rate of horizontal water transport, however, must always be a concern in any case. Note that serpentinization and thermal cracking should take place concurrently. At the very early stage of cracking, shallow cracks with narrow opening could easily be healed by serpentinization, and they would be repeatedly open by subsequent cracking and continuously healed by serpentinization only at shallow depths.

[52] This serpentinization restricted to shallow depths has an interesting dynamical consequence. It can effectively heal the cracked surface and trap deep water in the crack, which may raise the fluid pressure close to lithostatic. Though serpentinization itself does not lead to a notable reduction in the friction coefficient, such high fluid pressure can reduce considerably the "effective" friction coefficient, which is apparently needed for the generation of plate tectonics as discussed in Introduction.

[53] Furthermore, the confining pressure, which prevents the complete release of thermal stress, could vanish if the fluid pressure reaches lithostatic, and thermal cracking can continue further to release all of residual thermal stress. For mature oceanic lithosphere, for example, this secondary cracking could fracture down to $\sim$50 km (Figure 6), removing the stiff semibrittle core entirely (Figure 2). Because crack growth, serpentinization, and sediment infill could take place simultaneously and also continuously as the cooling of oceanic mantle proceeds, we must wait for future modeling studies to see if this secondary cracking is physically and chemically plausible.

[54] One important observation in this regard is the systematics of oceanic intraplate seismicity. Intraplate earthquakes in old oceanic lithosphere are mostly by thrust faulting [e.g., *Wiens and Stein*, 1983], which indicates that the ambient stress state must be compressional. Seafloor topography can provide such compressional stress (often called as "ridge push"), but its magnitude is up to only a few tens of MPa [e.g., *Dahlen*, 1981]. If residual thermal stress is not released by some mechanism, this compressional stress is completely overwhelmed by tensional thermal stress, which is greater by more than an order of magnitude. The number of intraplate earthquakes in old oceanic lithosphere is very small, so the observed systematics may not be statistically significant. However, if oceanic lithosphere is indeed predominantly in compression as has been believed for many years [e.g., *Sykes and Sbar*, 1973], some mechanism, such as secondary cracking due to shallow serpentinization, must exist to efficiently liberate residual thermal stress.

[55] My prediction for thermal cracking is global, not limited to any particular tectonic regimes. Thermal cracking must proceed continuously everywhere in ocean basins as oceanic lithosphere gradually cools down. The presence of surface water plays a critical role in my working hypothesis for weakening the stiffest part of lithosphere. Water has long been suspected to be somehow important for the operation of plate tectonics on Earth [e.g., *Tozer*, 1985; *Regenauer-Lieb et al.*, 2001], but its actual role remains rather vague. Though still speculative, my hypothesis is one plausible scenario for how water might help the generation of plate tectonics (or the spontaneous initiation of subduction), and at the very least, this study demonstrates that thermal stress can crack oceanic lithosphere, much more deeply than previously thought. My estimate of crack penetration depth involves only the well-established properties of shallow upper mantle: thermal expansivity, elastic constants, and mantle viscosity. Thus the possible physical and chemical

consequences of deep thermal cracking deserve careful consideration.

4.3. Further Implications and Possible Observational Tests

[56] The proposed mechanism for introducing water and thus damage into oceanic lithosphere is attractive for the generation of plate tectonics because weakness is already localized as the form of thermal cracks. How to localize deformation is not a major concern. The planform of these cracks is, however, yet to be investigated. Ridge-parallel cracks are certainly necessary to release ridge-parallel thermal stress, but if horizontal thermal stresses are close to isotropic in horizontal directions as the ridge-normal models suggest, other planforms such as hexagonal may be preferred. The planform of thermal cracks is expected to be affected by far-field tectonic stresses, so a variety of planforms may be possible. This planform issue is important also because of its connection to seismic anisotropy.

[57] My scenario of weakening lithosphere is accompanied with the structure of thermal crack system, and whatever this structure would be, it is unlikely to result in weakening lithosphere in all possible directions both vertically and horizontally. In other words, damaged lithosphere could be weak only for certain types of deformation and remain strong for others. This notion of anisotropic plate strength is probably important to explain the apparent dual nature of oceanic lithosphere, which should be strong enough to support the long-term loading of seamounts but should also be weak enough to bend relatively easily at subduction zones [e.g., *Gurnis et al.*, 2000]. I also note that seamount loading is more than mechanical loading. The emplacement of seamounts requires the migration of magma through lithosphere, which may affect the localized hydration and thus the strength of lithosphere.

[58] The deep hydration of oceanic lithosphere is likely to be important for other issues such as the origin of double seismic zones [e.g., *Peacock*, 2001; *Kerrick*, 2002] and the global water cycle [e.g., *Ito et al.*, 1983; *Jarrard*, 2003]. Deep (20–30 km) thermal cracks are formed with an interval of a few tens of kilometers, and each of these cracks have average opening of $\sim$50 m (Figure 6). The spatially averaged porosity is thus 0.1–0.2%. Combined with the present-day plate creation rate of $\sim$3 km^2 yr^{-1} [*Parsons*, 1982], such porosity suggests that the mantle contribution to global water flux at subduction zones may be $\sim$0.6–1.8 $\times$ 10^{14} g yr^{-1}, which is not trivial compared to the crustal contribution ($\sim$6 $\times$ 10^{14}g yr^{-1} [*Jarrard*, 2003]).

[59] Thermal stress modifies the structure of oceanic lithosphere by creating macroscopic cracks. If we can map out the geophysical structure of lithosphere with sufficiently high resolution, it would be a direct observational test of this study, but the fine-scale structure of oceanic lithosphere has been a blind spot in conventional geophysical remote sensing. Active source seismology with a dense array of ocean bottom seismometers can provide high-resolution image, but it is usually limited to crustal structure. Surface wave tomography can image deeper structure, but with much lower resolution. A recent study by *Lizarralde et al.* [2004], however, points to a promising direction. They demonstrated that, by repeating air gun firing and stacking resulting seismic profiles, one could enhance signal-to-noise ratio sufficiently high so that mantle refraction phases can be accurately identified. Their *P* wave velocity model for shallow mantle beneath old (>100-Ma-old) oceanic lithosphere exhibits a peculiar velocity gradient (Figure 11), which cannot be explained by a simple mantle column. Their preferred interpretation for this velocity gradient is the effect of trapped melt (and now frozen as gabbro) due to inefficient melt extraction processes at a slow spreading ridge. Interestingly, the depth extent for this high-velocity gradient is similar to what is predicted for the depth of thermal cracks. Though porosity due to thermal cracks is very low, seismic velocity is very sensitive to the shape of porosity, and crack-like porosity can considerably reduce seismic velocity even with this low porosity [e.g., *Korenaga et al.*, 2002, Figure 9b]. In any event, the high-resolution structure of oceanic lithosphere is now something we can reach for, and if we combine this new generation seismic acquisition with other geophysical methods such as magnetotelluric imaging, we should be able to distinguish between different hypotheses (e.g., failed melt migration vs. thermal cracking). Marine geophysics may provide a crucial key to resolving the generation of plate tectonics.

5. Conclusion and Outlook

[60] On the basis of viscoelastic thermal analysis, I have shown that thermal stress can deeply crack oceanic lithosphere, e.g., down to $\sim$30 km depth for 100-Ma-old lithosphere, and also that residual thermal stress is still tensional and on the order of a few hundred MPa, which has a potential to fracture mature oceanic lithosphere further down to $\sim$50 km depth. Earthquake studies suggest that oceanic lithosphere is generally under compression, which may indicate that secondary cracking due to shallow serpentinization could actually take place. The deep cracking of oceanic lithosphere has an inevitable chemical consequence, i.e., serpentinization, and its likely outcome is to create the localized zones of weakness in the stiffest part of lithosphere, which could facilitate the spontaneous initiation of subduction as well as self-sustained subduction and thus the generation of plate tectonics.

[61] This study is the first attempt to simulate thermal cracking in oceanic lithosphere, and the models are kept very simple. The main purpose is to demonstrate that thermal cracking can be very deep and thus thermal stress has a potential to affect the rheological evolution of oceanic lithosphere in a substantial manner. More elaborate models must be pursued in future, such as three-dimensional models to investigate the pattern of crack formation and physiochemical models to incorporate the effect of serpentinization. Some of the adopted boundary conditions may be debatable if one considers potential complications that may arise in the cracking (and healing) of real lithosphere, and such complications would be best handled in more elaborate models, for which the present study can serve as a baseline. Also, various tectonic processes that have been associated with thermal stress, including the seismicity of oceanic intraplate earthquakes, the spacing of transform faults, and lithospheric flexure, must be revisited carefully because the prevailing notion of thermal stress is likely to be incorrect. There are a number of theoretical tasks to be accomplished.

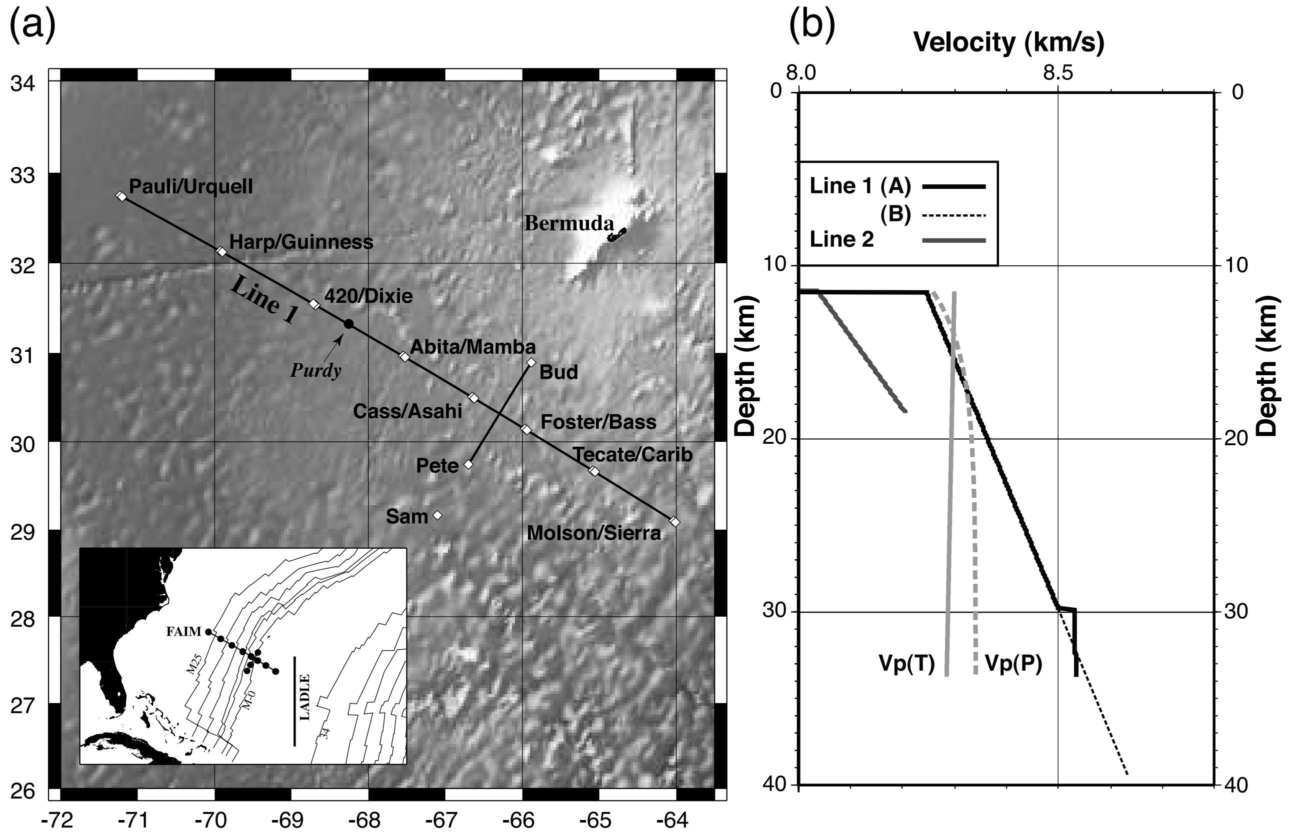

Figure 11. Seismic structure of old oceanic lithosphere according to the FAIM experiment (modified after *Lizarralde et al.* [2004], adapted with permission from Macmillan Publishers Ltd., copyright 2004). (a) Map of survey area with seismic lines. (b) *P* wave velocity model for the shallow upper mantle. Gray lines show velocity gradients expected for depleted mantle due to temperature and pressure effects. The actual velocity gradient (solid) constrained by the FAIM data is significantly greater than this predicted value, which may be due to failed melt migration as suggested by *Lizarralde et al.* [2004] or crack porosity (this study).

Equally exciting is that we now can probe the fine-scale geophysical structure of oceanic lithosphere, which should provide crucial observational clues.

Appendix A: Finite Element Implementation

[62] My construction of thermoviscoelastic finite element models is built on a standard finite element procedure for classical linear elastostatics. I thus begin with a brief review of this standard procedure, following *Hughes* [1987].

[63] A linear elastostatic problem is to find the displacement field u_i that satisfies all of the following:

$$\sigma_{ij,j} + f_i = 0 \quad \text{in} \quad \Omega \tag{A1}$$

$$u_i = g_i \quad \text{on} \quad \Gamma_{g_i} \tag{A2}$$

$$\sigma_{ij} n_j = h_i \quad \text{on} \quad \Gamma_{h_i} \tag{A3}$$

where Ω denotes the model domain without its boundary, Γ_{gi} is a part of the boundary on which displacement is prescribed, and Γ_{hi} is the rest of the boundary on which traction is prescribed. The unit outward normal vector to the boundary is denoted by n_i. This statement of the problem is referred to as the strong form in literature on the finite element method. For an isotropic case, the stress is defined in terms of the displacement as

$$\sigma_{ij} = \delta_{ij}\lambda u_{(k,k)} + 2\mu u_{(i,j)}, \tag{A4}$$

where

$$u_{(i,j)} \equiv \frac{u_{i,j} + u_{j,i}}{2}. \tag{A5}$$

[64] It can be shown that the above strong form is equivalent to the following weak form: Given f_i in Ω, g_i on Γ_{gi}, and h_i on Γ_{hi}, find $u_i \in \mathcal{S}_i$ such that for all $w_i \in \mathcal{V}_i$,

$$\int_\Omega w_{(i,j)}\sigma_{ij} d\Omega = \int_\Omega w_i f_i d\Omega + \sum_{i=1}^{n_d} \left(\int_{\Gamma_{h_i}} w_i h_i d\Gamma \right), \tag{A6}$$

where n_d is the number of dimensions, and σ_{ij} is defined in terms of u_i as in equation (4). The symbols $\mathcal{S}_i$ and $\mathcal{V}_i$ denote the trial solution space and the variation space, respectively.

Table B1. Numerical Errors For Transient Thermal Stress

$\eta(T)$	n = 32			n = 64			n = 128		
	N[a]	Average Error, %	Final Error, %	N	Average Error, %	Final Error, %	N	Average Error, %	Final Error, %
$\eta_0 = 10^{25}$ Pa s									
E = 100e3	170	0.44	0.62	650	0.20	0.60	2620	0.15	0.57
E = 300e3	170	0.42	0.64	650	0.21	0.65	2620	0.15	0.63
E = 600e3	170	0.42	0.69	650	0.21	0.71	2620	0.16	0.69
$\eta_0 = 10^{23}$ Pa s									
E = 100e3	460	2.77	1.69	640	0.73	0.60	2620	0.20	0.16
E = 300e3	440	1.26	0.64	640	0.33	0.24	2620	0.08	0.07
E = 600e3	400	1.06	0.47	640	0.22	0.17	2620	0.06	0.10
$\eta_0 = 10^{21}$ Pa s									
E = 100e3	46000	5.35	2.14	46000	1.61	1.05	46000	1.14	0.95
E = 300e3	44000	1.56	0.60	44000	0.54	0.34	44000	0.39	0.31
E = 600e3	40000	1.23	0.44	40000	0.42	0.25	40000	0.24	0.18

[a]Number of iterations required to reach t = 0.08.

Each member $u_i \in \mathcal{S}_i$ satisfies $u_i = g_i$ on Γ_{gi}, whereas each $w_i \in \mathcal{V}_i$ satisfies $w_i = 0$ on Γ_{gi}. By exploiting the fact that equation (6) must hold for all $w_i \in \mathcal{V}_i$, and by discretizing the continuous model space, one may arrive (after some algebra) at the following matrix equation:

$$K_{PQ} d_Q = F_P, \tag{A7}$$

where the stiffness matrix K_{PQ} depends on elastic constants, the displacement vector d_Q corresponds to the displacement field in Ω and on Γ_{hi}, and the force vector F_P depends on the external force f_i as well as the boundary values g_i and h_i. The indices P and Q run through all displacement nodes for all degrees of freedom excluding the boundary Γ_{gi}. By translating the strong form (second-order differential equation) to the weak form (first-order integrodifferential equation), the boundary conditions become a fictitious-force-like term, and in the special case of homogeneous boundary conditions, they are automatically satisfied because they make no contribution to F_P. Depending on model size and desired resolution, the stiffness matrix can be very large but also highly sparse, so the above matrix equation can be efficiently handled by common sparse matrix solvers. As my two-dimensional problems result in relatively small matrices, I use a direct solver based on Crout elimination [*Hughes*, 1987].

[65] Now I turn to the original viscoelastic problem. Equation (9) is approximated with the backward Euler algorithm as:

$$\begin{aligned}\frac{\sigma_{ij}^{n+1} - \sigma_{ij}^n}{\Delta t} + \frac{\sigma_{ij}^{n+1}}{\tau_r} = & \frac{2\mu}{\Delta t}\left(\varepsilon_{ij}^{n+1} - \varepsilon_{ij}^n\right) + 3\delta_{ij}\left[\frac{\lambda}{\Delta t}\left(\varepsilon^{n+1} - \varepsilon^n\right)\right. \\ & - \frac{\alpha_l K}{\Delta t}\left(\delta T^{n+1} - \delta T^n\right) \\ & \left. + \frac{K}{\tau_r}\left(\varepsilon^{n+1} - \alpha_l \delta T^{n+1}\right)\right],\end{aligned} \tag{A8}$$

where Δt is a time increment from time step n to $n + 1$, and τ_r is the relaxation timescale defined as η/μ. This may be arranged as:

$$\sigma_{ij}^{n+1} = \delta_{ij}\left[\lambda + (1-\gamma)\frac{2}{3}\mu\right]\Delta\varepsilon_{kk} + 2\gamma\mu\Delta\varepsilon_{ij} + \psi_{ij}^{n+1}, \tag{A9}$$

where

$$\psi_{ij}^{n+1} = -3\delta_{ij}\alpha_l K[\Delta T + (1-\gamma)\delta T^n] + \gamma\sigma_{ij}^n + \delta_{ij} K(1-\gamma)\varepsilon_{kk}^n, \tag{A10}$$

and

$$\gamma = \left(1 + \frac{\Delta t}{\tau_r}\right)^{-1}. \tag{A11}$$

[66] This is the time stepping algorithm for $n \geq 1$, with $\Delta\varepsilon_{ij} = \varepsilon_{ij}^{n+1} - \varepsilon_{ij}^n (= u_{(i,j)}^{n+1} - u_{(i,j)}^n)$ and $\Delta T = \delta T^{n+1} - \delta T^n$. The initial solution at $n = 0$ is provided by solving the following thermoelastic equilibrium (equation (1)):

$$\sigma_{ij}^0 = \delta_{ij}\lambda\varepsilon_{kk}^0 + 2\mu\varepsilon_{ij}^0 + \psi_{ij}^0, \tag{A12}$$

where

$$\psi_{ij}^0 = -3\delta_{ij}\alpha_l K \delta T. \tag{A13}$$

Starting with the initial solution u_i^0 and σ_{ij}^0, the displacement field is updated as $u_i^{n+1} = u_i^n + \Delta u_i$, and the corresponding stress field is calculated using equation (9).

[67] Note that both equations (9) and (12) share the same structure of the classical elastostatic equilibrium with a fictitious stress term ψ_{ij}. They are thus collectively treated in the following strong form statement: At the nth time step ($n \geq 0$), find $\tilde{u}_i^n$ that satisfies all of the following:

$$\sigma_{ij,j}^n = 0 \quad \text{in} \quad \Omega \tag{A14}$$

$$\tilde{u}_i^n = g_i^n \quad \text{on} \quad \Gamma_{g_i^n} \tag{A15}$$

$$\sigma_{ij}^n n_j = h_i^n \quad \text{on} \quad \Gamma_{h_i^n} \tag{A16}$$

where

$$\sigma_{ij}^n = \tilde{\sigma}_{ij}^n + \psi_{ij}^n, \tag{A17}$$

Table B2. Convergence Test for Crack Growth at 30-km Interval

Mesh Resolution	Crack Depth, km		
	t = 10 Ma	t = 50 Ma	t = 100 Ma
8 × 50	10	20	24
15 × 100	12	22	27
30 × 200	13	23.5	28
60 × 400	13.75	24	28.5

and

$$\widetilde{\sigma}_{ij}^{n} = \delta_{ij}\widetilde{\lambda}^{n}\widetilde{u}_{(k,k)}^{n} + 2\widetilde{\mu}^{n}\widetilde{u}_{(i,j)}^{n}. \quad (A18)$$

The definition of $\widetilde{u}_i^n$, $\widetilde{\lambda}^n$, and $\widetilde{\mu}^n$ is obvious from equations (9) and (12). A corresponding integrodifferential equation is

$$\int_\Omega w_{(i,j)}^n \widetilde{\sigma}_{ij}^n d\Omega = -\int_\Omega w_{(i,j)}^n \psi_{ij}^n d\Omega + \sum_{i=1}^{n_d}\left(\int_{\Gamma_{h_i^n}} w_i^n h_i^n d\Gamma\right), \quad (A19)$$

where w_i^n denotes a trial function that satisfies $\widetilde{u}_i^n = g_i^n$ on Γ_{gi}^n. From this, a matrix equation like equation (7) can be formulated to find (the discretized version of) $\widetilde{u}_i^n$.

[68] Bilinear quadrilateral elements are used, so the displacement field is defined at every node and continuous in Ω, but the stress field is defined only for each element as a whole and thus discontinuous from element to element. The least squares smoothing procedure [e.g., *Hughes* 1987, p. 227] is employed to assign stress at every node only for a displaying purpose. Stress should be kept element-wise when solving for $\widetilde{u}_{ij}^n$ with equation (19) or evaluating σ_{ij}^n using equation (9); otherwise, errors introduced by smoothing would quickly accumulate during time stepping. For each time step, viscosity is calculated for all elements using equation (10), and the time step Δt is chosen so that $\gamma \geq \gamma_{\min}$ for all elements. The benchmark test of my code is reported in Appendix B, which indicates that the code can stably track the temporal evolution of thermal stress when $\gamma_{\min} \geq 0.5$, which is equivalent to having $\Delta t \leq \tau_r$ everywhere. I used $\gamma_{\min}$ = 0.6 for all of my calculations.

Appendix B: Benchmark Test of Finite Element Code

[69] In order of verify my numerical code, two types of tests are conducted. For models without crack growth, an analytical solution exists for a simple viscosity model and one-dimensional temperature evolution [*Muki and Sternberg*, 1961], so this analytical solution is used as a benchmark. The solution by *Muki and Sternberg* [1961] may be better called semianalytical because it involves numerical integration, but this integration can easily be conducted to desired accuracy. For crack growth models, no analytical solution exists, and a convergence test is conducted instead.

[70] For no crack growth with one-dimensional temperature evolution, I use the temperature-dependent viscosity of Arrhenius type, i.e., $\eta(T) = \eta_0 \exp(E/RT - E/RT_0)$, where η_0 is the reference viscosity at $T = T_0$. Other model parameters are the same as in the main text. The numerical code is also implemented with a finite element solver for thermal diffusion, which is used to handle cooling other than simple half-space cooling (e.g., double-sided gradual cooling). Though half-space cooling is used in this benchmark test, the temperature field is nonetheless solved numerically to show the accuracy of the diffusion solver. The time increment is determined by either $\gamma_{\min}$ (set as 0.5 for this benchmark test) or the Courant time step for thermal diffusion, whichever smaller. As the depth extent of the model is only 100 km, tests were run up to the diffusion time of 0.08, after which the effect of the bottom boundary becomes significant in the temperature profile. The model domain was discretized by 1 × n elements, and I tested n = 32, 64, and 128. For temperature-dependent viscosity, I use all combinations of reference viscosities of 10^{21}, 10^{23}, and 10^{25} Pa s and activation energies of 100, 300, and 600 kJ mol^{-1}. As a measure of numerical error, I use root-mean-square difference in horizontal stress between numerical and analytical solutions (for $D/n < z \leq D$) scaled by the norm of the analytical solution, and report the average error for the entire model run as well as the error at the final time step. The shallowest element has the largest thermal stress but suffers most severely from errors in the temperature field for half-space cooling, so it is excluded from error calculation; otherwise the root-mean-square error would be unrepresentative of the rest of model domain. The benchmark comparison is reported in Table B1. Errors are less than 1% for most cases, and it is noted that the final error is in general very similar to the average error, indicating that error accumulation during time stepping is not a major source of numerical error. This is important because the number of time steps required for 100-Ma-long cooling is on the order of hundred thousands with the mantle rheology model.

[71] The crack growth model with 30-km spacing shown in Figure 6 is based on 15 × 100 elements. As a convergence test, I also tested 8 × 50, 30 × 200, and 60 × 400 elements. As the mesh resolution increases, stress singularity at the crack tip is more accurately modeled, which leads to greater crack depth. Results in terms of crack depth are compared in Table B2. The difference between the finest-resolution model and the standard model presented in Figure 6 is up to 2 km, and this degree of accuracy is sufficient for discussion in the main text.

[72] **Acknowledgments.** This work was sponsored by the U.S. National Science Foundation under grant EAR-0449517. This manuscript has benefited from official reviews by the Associate Editor Wouter Schellart, Slava Solomatov, and an anonymous reviewer. The author also thanks Dave Bercovici, Shun Karato, Tom Jordan, and Peter Kelemen, whose comments were helpful to improve the accuracy and clarity of the manuscript.

References

Anderson, T. L. (2005), *Fracture Mechanics: Fundamentals and Applications*, 3rd ed., Talyor and Francis, New York.
Ave Lallemant, H. G., J.-C. C. Mercier, N. L. Carter, and J. V. Ross (1980), Rheology of the upper mantle: inferences from peridotite xenoliths, *Tectonophysics*, *70*, 85–113.
Bercovici, D. (2003), The generation of plate tectonics from mantle convection, *Earth Planet. Sci. Lett.*, *205*, 107–121.
Bercovici, D., Y. Richard, and M. A. Richards (2000), The relation between mantle dynamics and plate tectonics: A primer, in *The History and Dynamics of Global Plate Motions*, *Geophys. Monogr. Ser.*, vol.121, edited by M. A. Richards, R. G. Gordon, and R. D. van der Hilst, pp. 5–46, AGU, Washington, D. C.
Bergman, E. A., and S. C. Solomon (1984), Source mechanisms of earthquakes near mid-ocean ridges from body waveform inversion: Implications for the early evolution of oceanic lithosphere, *J. Geophys. Res.*, *89*, 11,415–11,441.

Boley, B. A., and J. H. Weiner (1960), *Theory of Thermal Stresses*, John Wiley, Hoboken, N. J.

Bratt, S. R., E. A. Bergman, and S. C. Solomon (1985), Thermoelastic stress: How important as a cause of earthquakes in young oceanic lithosphere?, *J. Geophys. Res.*, *90*, 10,249–10,260.

Brudy, M., M. D. Zoback, K. Fuchs, F. Rummel, and J. Baumgartner (1997), Estimation of the complete stress tensor to 8 km depth in the KTB scientific drill holes: Implications for crustal strength, *J. Geophys. Res.*, *102*, 18,453–18,475.

Byerlee, J. D. (1978), Friction of rocks, *Pure Appl. Geophys.*, *116*, 615–626.

Carslaw, H. S., and J. C. Jaeger (1959), *Conduction of Heat in Solids*, 2nd ed., Oxford Univ. Press, New York.

Cloetingh, S., R. Wortel, and N. J. Vlaar (1989), On the initiation of subduction zones, *Pure Appl. Geophys.*, *129*, 7–25.

Conrad, C. P., and B. H. Hager (1999), The thermal evolution of an earth with strong subduction zones, *Geophys. Res. Lett.*, *26*, 3041–3044.

Dahlen, F. A. (1981), Isostasy and the ambient state of stress in oceanic lithosphere, *J. Geophys. Res.*, *86*, 7801–7807.

deMartin, B., G. Hirth, and B. Evans (2004), Experimental constraints on thermal cracking of peridotite at oceanic spreading centers, in *Mid-Ocean Ridges: Hydrothermal Interactions Between the Lithosphere and Oceans*, *Geophys. Monogr. Ser.*, vol.148, edited by C. R. German, J. Lin, and L. M. Parsons, pp. 167–185, AGU, Washington, D. C.

Denlinger, R. P., and W. Z. Savage (1989), Thermal stress due to cooling of a viscoelastic oceanic lithosphere, *J. Geophys. Res.*, *94*, 744–752.

Eiler, J. M. (2001), Oxygen isotope variations of basaltic lavas and upper mantle rocks, *Rev. Mineral.*, *43*, 319–364.

Evans, R. L., G. Hirth, K. Baba, D. Forsyth, A. Chave, and R. Mackie (2005), Geophysical evidence from the MELT area for compositional controls on oceanic plates, *Nature*, *437*, 249–252.

Fung, Y. C. (1965), *Foundations of Solid Mechanics*, Prentice-Hall, Upper Saddle River, N. J.

Gans, K. D., D. S. Wilson, and K. C. Macdonald (2003), Pacific Plate gravity lineaments: Diffuse extension or thermal contraction?, *Geochem. Geophys. Geosyst.*, *4*(9), 1074, doi:10.1029/2002GC000465.

Gardon, R. (1980), Thermal tempering of glass, in *Glass: Science and Technology*, vol. 5, *Elasticity and Strength in Glasses*, edited by D. R. Uhlmann and N. J. Kreidl, pp. 145–216, Elsevier, New York.

Goetze, C., and B. Evans (1979), Stress and temperature in the bending lithosphere as constrained by experimental rock mechanics, *Geophys. J. R. Astron. Soc.*, *59*, 463–478.

Gregory, R. T., and H. P. Taylor Jr. (1981), An oxygen isotope profile in a section of Cretaceous oceanic crust, Samail Ophiolite, Oman: Evidence for δ^{18}O buffering of the oceans by deep (>5 km) seawater-hydrothermal circulation at mid-ocean ridges, *J. Geophys. Res.*, *86*, 2737–2755.

Gurnis, M., S. Zhong, and J. Toth (2000), On the competing roles of fault reactivation and brittle failure in generating plate tectonics from mantle convection, in *The History and Dynamics of Global Plate Motions*, *Geophys. Monogr. Ser.*, vol. 121, edited by M. A. Richards, R. G. Gordon, and R. D. van der Hilst, pp. 73–94, AGU, Washington, D. C.

Gurnis, M., C. Hall, and L. Lavier (2004), Evolving force balance during incipient subduction, *Geochem. Geophys. Geosyst.*, *5*, Q07001, doi:10.1029/2003GC000681.

Hager, B., and R. O'Connell (1978), Subduction zone dip angles and flow driven by plate motion, *Tectonophysics*, *50*, 111–133.

Haxby, W. F., and E. M. Parmentier (1988), Thermal contraction and the state of stress in the oceanic lithosphere, *J. Geophys. Res.*, *93*, 6419–6429.

Hirth, G., and D. L. Kohlstedt (1996), Water in the oceanic mantle: Implications for rheology, melt extraction, and the evolution of the lithosphere, *Earth Planet. Sci. Lett.*, *144*, 93–108.

Hirth, G., and D. Kohlstedt (2003), Rheology of the upper mantle and the mantle wedge: A view from the experimentalists, in *Inside the Subduction Factory*, *Geophys. Monogr. Ser.*, vol. 138, edited by J. Eiler, pp. 83–105, AGU, Washington, D. C.

Hughes, T. J. R. (1987), *The Finite Element Method: Linear Static and Dynamic Finite Element Analysis*, Prentice-Hall, Upper Saddle River, N. J.

Ito, E., D. M. Harris, and A. T. Anderson (1983), Alteration of oceanic crust and geologic cycling of chlorine and water, *Geochim. Cosmochim. Acta*, *47*, 1613–1624.

Jarrard, R. D. (2003), Subduction fluxes of water, carbon dioxide, chlorine, and potassium, *Geochem. Geophys. Geosyst.*, *4*(5), 8905, doi:10.1029/2002GC000392.

Karato, S., and H. Jung (2003), Effects of pressure on high-temperature dislocation creep in olivine, *Philos. Mag.*, *83*, 401–414.

Karato, S., and P. Wu (1993), Rheology of the upper mantle: A synthesis, *Science*, *260*, 771–778.

Karato, S.-I. (1998), Micro-physics of post glacial rebound, *GeoRes. Forum*, *3–4*, 351–364.

Karato, S.-I., M. Paterson, and J. D. Fitzgerald (1986), Rheology of synthetic olivine aggregates: Influence of grain size and water, *J. Geophys. Res.*, *91*, 8151–8176.

Kemp, D., and D. Stevenson (1996), A tensile flexural model for the initiation of subduction, *Geophys. J. Int.*, *125*, 73–94.

Kerrick, D. (2002), Serpentinite seduction, *Science*, *298*, 1344–1345.

Kohlstedt, D. L., B. Evans, and S. J. Mackwell (1995), Strength of the lithosphere: Constraints imposed by laboratory experience, *J. Geophys. Res.*, *100*, 17,587–17,602.

Korenaga, J. (2003), Energetics of mantle convection and the fate of fossil heat, *Geophys. Res. Lett.*, *30*(8), 1437, doi:10.1029/2003GL016982.

Korenaga, J. (2006), Archean geodynamics and the thermal evolution of Earth, in *Archean Geodynamics and Environments*, *Geophys. Monogr. Ser.*, vol.164, edited by K. Benn, J.-C. Mareschal, and K. Condie, pp. 7–32, AGU, Washington, D. C.

Korenaga, J., P. B. Kelemen, and W. S. Holbrook (2002), Methods for resolving the origin of large igneous provinces from crustal seismology, *J. Geophys. Res.*, *107*(B9), 2178, doi:10.1029/2001JB001030.

Lachenbruch, A. H. (1961), Depth and spacing of tension cracks, *J. Geophys. Res.*, *66*, 4273–4292.

Lachenbruch, A. H., and J. Sass (1980), Heat flow and energetics of the San Andreas fault zone, *J. Geophys. Res.*, *85*, 6185–6222.

Lawn, B. R., and T. R. Wilshaw (1975), *Fracture of Brittle Solids*, Cambridge Univ. Press, New York.

Lee, E. H., T. G. Rogers, and T. C. Woo (1965), Residual stresses in a glass plate cooled symmetrically from both surfaces, *J. Am. Ceram. Soc.*, *53*, 480–487.

Lizarralde, D., J. B. Gaherty, J. A. Collins, G. Hirth, and S. D. Kim (2004), Spreading-rate dependence of melt extraction at mid-ocean ridges from mantle seismic refraction data, *Nature*, *432*, 744–747.

McKenzie, D. (1977), The initiation of trenches: A finite amplitude instability, in *Island Arcs, Deep Sea Trenches and Back-Arc Basins*, *Maurice Ewing Ser.*, vol.1, edited by M. Talwani and W. C. Pitman III, pp. 58–61, AGU, Washington, D. C.

Moresi, L., and V. Solomatov (1998), Mantle convection with a brittle lithosphere: thoughts on the global tectonic styles of the Earth and Venus, *Geophys. J. Int.*, *133*, 669–682.

Muki, R., and E. Sternberg (1961), Transient thermal stresses in viscoelastic materials with temperature dependent properties, *J. Appl. Mech.*, *28*, 193–207.

Narayanaswamy, O. S., and R. Gardon (1969), Calculation of residual stress in glass, *J. Am. Ceram. Soc.*, *52*, 554–558.

Parmentier, E. M., and W. F. Haxby (1986), Thermal stresses in the oceanic lithosphere: Evidence from geoid anomalies at fracture zones, *J. Geophys. Res.*, *91*, 7193–7204.

Parsons, B. (1982), Causes and consequences of the relation between area and age of the ocean floor, *J. Geophys. Res.*, *87*, 289–302.

Peacock, S. M. (2001), Are the lower planes of double seismic zones caused by serpentine dehydration in subducting oceanic mantle?, *Geology*, *29*, 299–302.

Ranero, C. R., J. P. Morgan, K. McIntosh, and C. Reichert (2003), Bending-related faulting and mantle serpentinization at the Middle America trench, *Nature*, *425*, 367–373.

Regenauer-Lieb, K., D. A. Yuen, and J. Branlund (2001), The initiation of subduction: Criticality by addition of water?, *Science*, *294*, 578–580.

Richards, M. A., W. Yang, J. R. Baumgardner, and H. Bunge (2001), Role of a low-viscosity zone in stabilizing plate tectonics: Implications for comparative terrestrial planetology, *Geochem. Geophys. Geosyst.*, *2*(8), doi:10.1029/2000GC000115.

Sandwell, D., and Y. Fialko (2004), Warping and cracking of the Pacific plate by thermal contraction, *J. Geophys. Res.*, *109*, B10411, doi:10.1029/2004JB003091.

Sandwell, D. T. (1986), Thermal stress and the spacing of transform faults, *J. Geophys. Res.*, *91*, 6405–6417.

Schellart, W. P., G. S. Lister, and V. G. Toy (2006), A Late Cretaceous and Cenozoic reconstruction of the southwest Pacific region: Tectonics controlled by subduction and slab rollback processes, *Earth Sci. Rev.*, *76*, 191–233.

Scholz, C. H. (2000), Evidence for a strong San Andreas fault, *Geology*, *28*, 163–166.

Scholz, C. H. (2002), *The Mechanics of Earthquakes and Faulting*, 2nd ed., Cambridge Univ. Press, New York.

Schubert, G., D. L. Thurcotte, and P. Olson (2001), *Mantle Convection in the Earth and Planets*, Cambridge Univ. Press, New York.

Solomatov, V. S. (1995), Scaling of temperature- and stress-dependent viscosity convection, *Phys. Fluids*, *7*, 266–274.

Solomatov, V. S. (2004), Initiation of subduction by small-scale convection, *J. Geophys. Res.*, *109*, B01412, doi:10.1029/2003JB002628.

Stein, C., J. Schmalzl, and U. Hansen (2004), The effect of rheological parameters on plate behaviour in a self-consistent model of mantle convection, *Phys. Earth Planet. Inter.*, *142*, 225–255.

Stern, R. J. (2004), Subduction initiation: Spontaneous and induced, *Earth Planet. Sci. Lett.*, *226*, 275–292.
Sykes, L. R., and M. L. Sbar (1973), Intraplate earthquakes, lithospheric stresses and the driving mechanism of plate tectonics, *Nature*, *245*, 298–302.
Tackley, P. J. (2000), Mantle convection and plate tectonics: Toward an integrated physical and chemical theory, *Science*, *288*, 2002–2007.
Tozer, D. C. (1985), Heat transfer and planetary evolution, *Geophys. Surv.*, *7*, 213–246.
Turcotte, D. L. (1974), Are transform faults thermal contraction cracks?, *J. Geophys. Res.*, *79*, 2573–2577.
Turcotte, D. L., and E. R. Oxburgh (1973), Mid-plate tectonics, *Nature*, *244*, 337–339.
Turcotte, D. L., and G. Schubert (1982), *Geodynamics: Applications of Continuum Physics to Geological Problems*, John Wiley, Hoboken, N. J.
Wedepohl, H. (1995), The composition of the continental crust, *Geochim. Cosmochim. Acta*, *59*, 1217–1239.
Weertman, J. (1970), The creep strength of the Earth's mantle, *Rev. Geophys.*, *8*, 146–168.
Weinstein, S. A., and P. Olson (1992), Thermal convection with non-Newtonian plates, *Geophys. J. Int.*, *111*, 515–530.
Wessel, P. (1992), Thermal stresses and the bimodal distribution of elastic thickness estimates of the oceanic lithosphere, *J. Geophys. Res.*, *97*, 14,177–14,193.
Wessel, P., and W. F. Haxby (1990), Thermal stresses, differential subsidence, and flexure at oceanic fracture zones, *J. Geophys. Res.*, *95*, 375–391.
Wiens, D. A., and S. Stein (1983), Age dependence of oceanic intraplate seismicity and implications for lithospheric evolution, *J. Geophys. Res.*, *88*, 6455–6468.
Wiens, D. A., and S. Stein (1984), Intraplate seismicity and stresses in young oceanic lithosphere, *J. Geophys. Res.*, *89*, 11,442–11,464.
Wilson, J. T. (1966), Did the Atlantic close and then re-open?, *Nature*, *211*, 676–681.

J. Korenaga, Department of Geology and Geophysics, P.O. Box, 208109, Yale University, New Haven, CT 06520-8109, USA. (jun.korenaga@yale.edu)